

Master Thesis

**How to Distribute New Solar Systems in Europe to Reduce Power Production
Variability**

Department Environmental Systems Science / Earth Sciences, ETH Zürich

Institute for Atmospheric and Climate Science

Supervisors:

Dr. Jan Wohland, Institute for Environmental Decisions, ETH Zürich

Dr. Doris Sylvia Folini, Institute for Atmospheric and Climate Science, ETH Zürich

Dr. Stefan Pfenninger, Faculty of Technology, Policy and Management, TU Delft

Prof. Dr. Martin Wild, Institute for Atmospheric and Climate Science, ETH Zürich

Submitted by

Dirk Mühlemann

13-732-037

Uster, 24/04/2021

Acknowledgement

First and foremost, I would like to show my greatest appreciation to Dr. Jan Wohland, Dr. Doris Folini and Dr. Stefan Pfenninger for the ongoing assistance and illuminating discussions throughout my research. Without their guidance and help, this thesis would not have been possible. I thank Prof. Dr. Martin Wild for the opportunity to write this thesis as a co-operation between the Institute for Atmospheric and Climate Science and the Institute for Environmental Decisions. Finally, I want to thank my wife and children. I could not have completed this thesis without their support.

Abstract

To reduce greenhouse gas emissions and combat climate change, the electrical power production sector faces a fundamental transition from conventional fossil to renewable technologies. The transition has already started, which can be seen by the effort and ambitious targets of many nations worldwide. Installed solar photovoltaics (PV) capacities are increasing every year and currently produce around 5.5% of the European electricity demand. Since PV power production depends on weather and climate, it exhibits a highly variable production pattern that typically differs from consumption patterns in space and time. One concrete challenge concerns electricity grids because their stability depends on balanced supply and demand. Further deployment of PV systems as foreseen for 2030 in the National Energy and Climate Plans could increase variability and further add to this challenge.

This study presents spatial distributions of newly installed PV systems in Europe that minimize the multiday power production variability due to changing weather regimes. The latter are identified via empirical orthogonal functions (EOFs) with subsequent k-mean clustering, applied to the 500 hPa geopotential height field in the ERA5 reanalysis data, 1979 to 2020. Using country-specific PV capacity factors (hourly data, provided by Renewables.ninja, 1985 to 2016) and installed capacities, we arrive at quantitative PV production estimates per country, weather regime (seven in total), and season. We examine associate over- and underproduction for current and planned (2030 and 2050) installed capacities and show that a more even PV production is possible with alternative spatial distributions of installed capacities.

Upon transition from one weather regime to another, current total PV production in Europe varies by 0.9 GW on average with a maximum change of 3.0 GW. We report that with the planned installed PV capacity distribution, these values roughly triple by 2030, to 2.7 GW and 8.5 GW, respectively. For 2050, a range of planned installed PV capacity distributions were examined, yielding PV production changes of 6.4 GW to 63.2 GW on average, with maximum changes upon weather regime transition between 20.1 GW and 198.6 GW. Optimizing the spatial distribution of future installed capacities based on climate information, these variabilities can be reduced by roughly 30%. This yields a reduction of maximum changes of roughly 60 GW in 2050. To put this in context, to balance the power grid, we would save up to about 60 nuclear power plants worth of electricity. The variability reduction could be achieved by placing the new installed PV capacity to mainly South-eastern and North-western Europe. Our work is a crucial example of why the spatial distribution of PV systems should be carefully considered and coordinated with other renewable technologies, storage possibilities, and transmission before deployment.

Abbreviations

| | |
|-----------------|---|
| CF | Capacity Factor |
| DJF | December, January, February |
| ECMWF | European Centre for Medium-Range Weather Forecasts |
| ENTSO-E | European Network of Transmission System Operators for Electricity |
| EOF | Empirical Orthogonal Function |
| ERA | ECMWF Reanalysis |
| EU | European Union |
| Eurostat | Statistical office of the European Union |
| GSEE | Global Solar Energy Estimator |
| IC | Installed capacities |
| IRENA | International Renewable Energy Agency |
| JJA | June, July, August |
| MAM | March, April, May |
| MERRA | Modern-Era Retrospective analysis for Research and Applications |
| NAO | North Atlantic Oscillation |
| NECPs | National Energy and Climate Plans |
| OPSD | Open Power System Data |
| PV | Photovoltaics |
| S1 - S4 | Scenario 1 - Scenario 4 |
| SARAH | Surface Solar Radiation Data Set - Heliosat |
| SON | September, October, November |
| WR | Weather Regime |

Contents

| | | |
|-------|---|----|
| 1. | Introduction | 1 |
| 2. | Data & Methods | 4 |
| 2.1 | Data | 4 |
| 2.1.1 | ERA5 | 4 |
| 2.1.2 | Renewables.ninja and Global Solar Energy Estimator (GSEE) | 4 |
| 2.1.3 | Installed PV capacities | 7 |
| 2.1.4 | Electricity consumption data | 8 |
| 2.2 | Method..... | 10 |
| 2.2.1 | Weather regime classification | 10 |
| 2.2.2 | Capacity factors and PV power production variability | 12 |
| 2.2.3 | Variability reduction with optimized installed PV capacity distribution | 13 |
| 2.2.4 | Scenarios | 14 |
| 3. | Results | 18 |
| 3.1 | Weather regimes and their linked capacity factor anomalies | 18 |
| 3.1.1 | Weather regime 0 - NAO+ | 22 |
| 3.1.2 | Weather regime 1 - European trough | 22 |
| 3.1.3 | Weather regime 2 – NAO- | 23 |
| 3.1.4 | Weather regime 3 - Atlantic ridge | 23 |
| 3.1.5 | Weather regime 4 - Atlantic trough..... | 23 |
| 3.1.6 | Weather regime 5 - European blocking..... | 24 |
| 3.1.7 | Weather regime 6 - Scandinavian blocking..... | 24 |
| 3.1.8 | No regime | 24 |
| 3.2 | Installed capacity distributions and their variability..... | 25 |
| 3.2.1 | Scenario 1 – Retain PV power production in 2030, but reduce variability | 26 |
| 3.2.2 | Scenario 2 – Retain PV power production in 2050, but reduce variability | 30 |
| 3.2.3 | Scenario 3 – Cost and variability minimization | 33 |

| | |
|---|----|
| 3.2.4 Scenario 4 – Coverage of country-specific electricity consumption | 34 |
| 4. Discussion | 39 |
| 4.1 Comparison to past work..... | 39 |
| 4.1.1 Weather regimes classification..... | 39 |
| 4.1.2 Capacity factor anomalies and surface weather variables | 40 |
| 4.1.3 Current and projected PV power production variability | 42 |
| 4.2 Dangers of increased variability..... | 43 |
| 4.3 Opportunities to decrease variability | 45 |
| 4.3.1 Scenario 1 – Retain PV power production in 2030, but reduce variability | 45 |
| 4.3.2 Scenario 2 – Retain PV power production in 2050, but reduce variability | 46 |
| 4.3.3 Scenario 3 – Cost and variability minimization | 47 |
| 4.3.4 Scenario 4 – Coverage of country-specific electricity consumption..... | 47 |
| 4.4 Limitations..... | 48 |
| 5. Conclusion & Outlook..... | 49 |
| 6. References | 51 |
| 7. Appendix | 53 |
| 8. Declaration of originality | 62 |

1. Introduction

Many governments undertake ambitious climate mitigation efforts to reduce the adverse effect of global warming and thereby try to meet the maximum warming target of 1.5°C from the Paris agreement (Hulme, 2016). A transition from conventional fossil to renewable energy technologies is substantial to achieve this goal. Solar power generating photovoltaic (PV) systems, as one of the major renewable technologies, have seen tremendous growth in recent years. According to the PV status report (2019) by the European Commission, there was a global installed capacity of 520 GW by the end of 2018 (Jäger-Waldau, 2019). By the end of 2019, the installed capacity was expected to reach 650 GW, which allows the PV systems to produce roughly 4% of the global electricity demand. Europe's share of installed PV capacity at the end of 2018 was about 117 GW, producing 5.5% of the electricity demand. Current scenarios for the required amount of installed PV capacity to reach a global 100% renewable electricity production in 2050 suggest that the capacity must rise to more than 4 TW by 2025 and 21.9 TW by 2050. For Europe, this would imply a PV installed capacity of 630 GW by 2025 and 1.94 TW by 2050 (Jäger-Waldau, 2019). Current (2019) planning strategies by the Nation Energy and Climate Plans (NECPs) of the European Union (EU) suggest that the installed PV capacity will increase to 387 GW by 2030. This is less than proposed by Jäger-Waldau (2019) but still shows the intention to grow and the additional effort needed towards 2050.

Available surface solar radiation and panel temperature dominate a PV panel's efficiency (Huld et al., 2010). Since these two variables are related to large-scale weather regimes (WRs), the PV power production is subject to significant fluctuations. The PV (and wind) power production pattern varies substantially from one WR to another (Drücke et al., 2020; Graabak & Korpås, 2016; Stram, 2016). To operate a stable power grid, electricity consumption must always equal electricity production. If the production is higher than the consumption, the power grid frequency increases, which can cause damage to connected electrical devices. If the consumption is higher than the production, the frequency decreases, leading to power outages (Hirth & Ziegenhagen, 2015). The increase of wind and PV installed capacities requires accurate forecasting of renewable power production to balance the power grid. Therefore, the knowledge of WRs and their impact on renewable energy production patterns is essential.

There are different approaches to classify WRs. The most common is based on empirical orthogonal function (EOF) analyses and k-mean clustering with 500 hPa geopotential height anomalies (Cassou, 2008; Michelangeli et al., 1995). Different studies have used this approach to determine power production variability with renewable (wind and PV) energy technologies (Brayshaw et al., 2011; Ely et al., 2013; Grams et al., 2017; van der Wiel et al., 2019). Another approach is to include the renewable electricity production and electricity demand with the weather variables to define 'Targeted Circulation Types' that determine the WR that influences the energy system the most (Bloomfield et al., 2020). Others expand the analysis to initially subjectively defined 29 Grosswetterlagen developed by Baur et al. (1944) to assess the

energy system's stress caused by renewable power production variability and electricity demand (Jones et al., 2020). The focus of current literature is mainly on wind power production in winter. This arises from the fact that wind power production variability is currently dominating over PV power production variability (Grams et al., 2017). Furthermore, the weather regime classification is usually done for winter, when the electricity demand is highest in Europe, increasing the energy system's stress (van der Wiel et al., 2019). This has led to the four well-known weather regimes (positive and negative phase of the North Atlantic Oscillation, Scandinavian blocking, and Atlantic ridge) and their impact on the energy system in winter is very well researched.

Fewer studies have tried to classify WRs year-round and to assess the renewable power production variability over the whole year (Grams et al., 2017). Projections to the future, especially for WR-driven PV power production variability and its possible impacts, are less well researched. With global warming, the electricity demand in the European summer increases because energy is used for cooling purposes. Thus stress for the energy system is increasing in summer, highlighting the need to expand analysis from winter to summer (Jakubcjonis & Carlsson, 2017). Furthermore, wind turbines and solar systems' growth increases the stress for the energy system caused by variable power production patterns in all seasons. A year-round analysis with possible future scenarios is crucial to fill this knowledge gap.

To our knowledge, there is only one study investigating the potential of reducing renewable power production variability with an optimized distribution of wind fleets or PV systems within Europe based on weather regime classification. Grams *et al.* (2017) concluded that spatial deployment of wind fleets based on weather regime information could reduce the wind power production variability within Europe substantially. They also analysed the PV power production variability. However, they did not further investigate it because their findings indicate that it would need a tenfold increase of installed PV capacity in Europe to be comparable to wind power production variability. Even though the decision to focus on wind rather than solar power output variability is understandable, calculations of necessary future installed PV capacities give reason to do the investigations anyway. Manish Ram *et al.* (2017) estimate that installed PV capacity for a 100% renewable scenario in Europe must rise to 1.94 TW by 2050. The International Renewable Energy Agency (IRENA) estimate Europe's share a bit lower to 0.89 TW. This is roughly a ten to twentyfold increase of installed PV capacity compared to the 87.19 GW installed PV capacity used in the study by Grams *et al.* (2017). Therefore, the impact of multiday PV power production variability caused by different WRs could become substantially more important, which makes the timely investigation of an optimized spatial deployment of future PV systems in Europe in advance of widespread PV deployments of great interest. The results could support current planning activities and reduce future balancing problems of the power grid. Furthermore, the distribution of wind fleets, which reduces the wind power production variability obtained by Grams *et al.* (2017), is not the result of a formal optimization. A more sophisticated

method that numerically finds a distribution of PV systems that reduces PV power production variability could easily be extended to wind power production variability.

This study aims to provide potential locations for new PV systems in Europe to reduce the PV power production variability. The study region will be based on geographical coverage and extent of the European network of transmission system operators for electricity (ENTSO-E), including 36 countries. We first focus on the current PV power production variability within Europe. Second, a projection of the PV power production variability to the year 2030 is made by considering the current plans from the NECPs. Third, different scenarios for 2050 are analysed to highlight where the variability could lead to. Finally, we introduce a method that numerically finds a distribution of PV systems that reduces the power production variability. A key element of the method is the ease of expansion, including wind power production variability and other constraints that must be fulfilled.

2. Data & Methods

Here, the data sources used in this study are introduced, and the approach to estimate current and future PV power production variability is described. Finally, we present a method that finds a distribution of PV systems that reduces the PV power production variability in Europe.

2.1 Data

2.1.1 ERA5

The reanalysis dataset, [ERA5](#) (Hersbach et al., 2018), published by the European Centre for Medium-Range Weather Forecasts (ECMWF), is used as the source for the weather regime definition. It provides atmospheric, land and oceanic variables from 1979 to the present with a temporal resolution of an hour. The grid of ERA5 has a horizontal spatial resolution of 0.28 degrees (~31km) and 37 pressure levels in the vertical. Detailed documentation about the ERA5 reanalyses dataset can be found on the ECMWF confluence web page (Hennermann & Yang, 2018).

We use the 500 hPa geopotential height variable from ERA5 in the domain 80°W to 40°E, 30°N to 90°N, covering the North Atlantic and continental Europe. Geopotential height is related to low and high-pressure systems (cyclones/anticyclones) and therefore to weather systems. Thus, they are commonly used for weather regime classification (Cassou, 2008; Grams et al., 2017; Michelangeli et al., 1995). The domain specification is reasonable for our meteorological field investigations since it captures the largescale circulation that affects Europe. The hourly dataset covers the time from 01.01.1979 to 31.05.2020, which yields 363'048 data points. Additionally, the [ERA5-Land](#) (Muñoz Sabater, 2019) hourly data from 01.01.1981 to 31.05.2020 are used to get an overview of 2m temperature and surface solar radiation of the classified weather regimes. It is explicitly designed for surface application and provides a more accurate dataset for this framework. Over complex terrain (orography), the ERA5-Land adds value to the ERA5 surface field. Furthermore, ERA5-Land has a higher spatial resolution of 0.1 degrees (~9km) (Muñoz Sabater, 2019). We choose a slightly coarser resolution of 0.25 degrees, comparable to the 0.28 degrees resolution of geopotential height.

2.1.2 Renewables.ninja and Global Solar Energy Estimator (GSEE)

[Renewables.ninja](#) (www.renewables.ninja) is an interactive web platform that simulates hourly power production of wind and solar power plants worldwide. It uses the so-called Global Solar Energy Estimator (GSEE) to calculate the PV power production. The source code of GSEE is freely available on [GitHub](#), and a detailed description of GSEE can be found in Pfenninger and Staffell (2016). The study by Huld *et al.* (2010) is the theoretical background of GSEE. The following variables are the key meteorological input parameters required to estimate the energy yield of PV modules:

1. Direct and diffuse irradiance at the PV panel

2. Panel temperature

Pfenninger and Staffell (2016) use three data sources to estimate these variables: The two reanalysis datasets of Modern-Era Retrospective analysis for Research and Applications (MERRA and MERRA-2) and the Surface Solar Radiation Data Set - Heliosat (SARAH). Figure 1 shows the general approach of GSEE, and the following paragraph further explains it. We use the dataset from Renewables.ninja based on the reanalyse dataset MERRA-2 covering 1985-2016. Hereafter, the differences between the datasets and their advantages and disadvantages are described to justify its use.

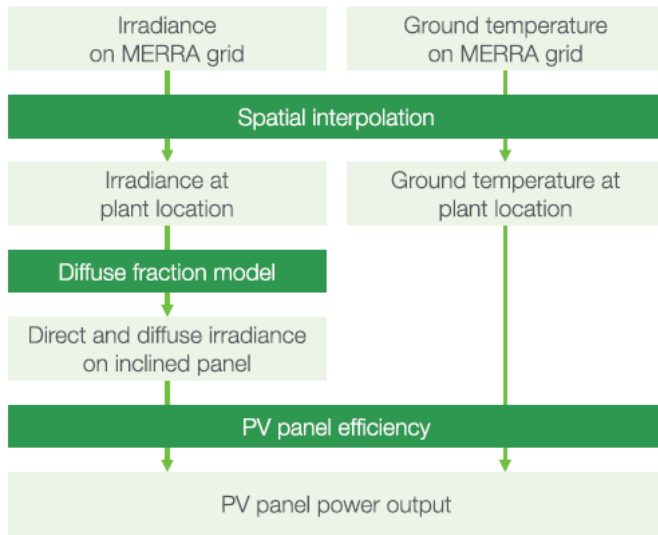


Figure 1: Overview of the approach used to model PV power production (Pfenninger & Staffell, 2016).

Since the estimates with MERRA are no longer provided by Renewables.ninja we will only discuss the two datasets MERRA-2 and SARAH. Both are provided in hourly intervals from 1985-2016. SARAH is a satellite-derived irradiance dataset with a high spatial resolution of $0.05^\circ \times 0.05^\circ$, whereas MERRA-2 is a reanalysis dataset with a lower spatial resolution of 0.5° latitude and 0.625° longitude. MERRA-2 only provides direct irradiance, but diffuse irradiance is needed as well. Therefore, Pfenninger and Staffell (2016) use the Boland-Ridley-Lauret model to estimate the diffuse irradiance (Ridley *et al.* 2010; Lauret *et al.* 2013). Since SARAH provides direct and global irradiance, no further estimates are needed.

Additionally, they use 2m air temperature from MERRA-2 as estimates for the ambient temperature. To get the panel temperature, they use the ambient temperature of MERRA-2 and additionally consider the effect of the irradiance on panel temperature. This relation was estimated with site measurements of one of their sources (DTI see below). This dataset provides ambient and panel temperature for each site with which they derived an empirical relationship.

It is more common and easier to compare and analyse PV power production with capacity factors (CF) than with absolute power production, and we use this approach as well. It is also used by Pfenninger and Staffell (2016), which is why we introduce it here to be able to discuss their results. The unit-less capacity factor is defined as:

$$CF = \frac{P}{IC} \quad \text{Eq. 1}$$

where P is power production [W] and IC is the installed capacity [W]. Power production P is defined as the net electricity output (in our case generated with PV systems) over a given time. The installed capacity (IC) is defined as the maximum possible electricity output (under optimal conditions) over that time. A CF of one is achieved when a PV system always produces electricity under optimal conditions during the time under review. A CF of zero indicates that no electricity is produced. The average yearly CF of PV systems in European countries is roughly between 0.1 and 0.2.

Pfenninger and Staffell (2016) compared their theoretical derived results with capacity factors based on on-site measurements. To get the measured capacity factors, they used three sources: DTI, PVLog.de and PVOutput.org. Over 1000 site data (measurements from PV systems) were collected from these three sources. Figure 2 shows a histogram of the difference between measured capacity factors and capacity factors simulated with GSEE.

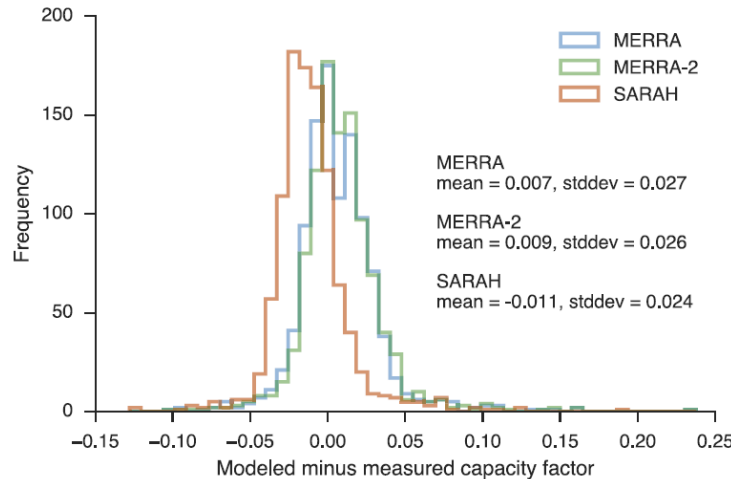


Figure 2: Histogram of the difference between the three modelled and measured capacity factors. Negative values infer underestimations of the capacity factor, and positive values infer overestimation. The blue graph corresponds to modelled data with MERRA, the green graph to MERRA-2 and the red graph to SARAH. (Pfenninger and Staffell, 2016)

Pfenninger and Staffell (2016) take the mean of these differences as the basis for a bias correction. They use it to calculate one correction factor for each simulation (MERRA-2 and SARAH).

In addition to the power output simulation of a wind or solar plant at a specific location, Renewables.ninja also provides capacity factors per country. Pfenninger and Staffell (2016) have performed randomized (tilt and azimuth angle) national-scale simulations with MERRA-2 and SARAH data to estimate averaged

capacity factors per country. These data were analysed against the measured site data. The measured capacity factor per country was then calculated as the mean of all capacity factors per site in one country. This capacity factor per country perfectly suits our need for analysing large-scale PV power production variability and its reduction potential.

Since our study focuses on reducing PV power production variability within Europe, we operate with relatively large-scale and long-term quantities. Therefore, we use the country-specific capacity factors derived with the reanalysis dataset MERRA-2. The reason to choose MERRA-2 rather than SARAH is its long-term consistency. According to Pfenninger and Staffell (2016), SARAH suffers from a significant amount of missing data. They state that, especially before 1995, the lack of data prevents long-term consistency. SARAH's benefits would be the higher spatial resolution and higher precision in estimating the energy yield of PV panels on hourly to daily time scales, which is not crucial for our analysis. Nevertheless, an advantage of this approach is to be in line with the study of Grams *et al.* (2017), which makes further comparison or combined analyses of wind and solar power output variability easier.

2.1.3 Installed PV capacities

Data from the International Renewable Energy Agency (IRENA) are used to gather the currently installed PV capacities (2019) for each country in Europe (Table 2). *"IRENA is an intergovernmental organisation that supports countries in their transition to a sustainable energy future, and serves as the principal platform for international co-operation, a centre of excellence, and a repository of policy, technology, resource and financial knowledge on renewable energy"* (IRENA, 2020b, p. 2). With the capacity factors by Renewables.ninja (section 2.1.2), each country's PV power production is calculated (Eq. 1).

To analyse where the PV power production variability is heading, the National Energy and Climate Plans (NECPs) of each country in the EU is used. Within the NECPs, each country defines the number of PV systems they plan to install until 2030. For the rest of Europe, individual national plans are considered or, if not available, the average PV installed capacity growth rate until the year 2030 from all EU countries is multiplied with the currently installed PV capacity to get an estimate. An overview of the data used can be found in Table 2, page 9.

Furthermore, the estimates where we need to be by 2050 presented in the "Energy Transformation Roadmap to 2050" by IRENA are used as one source for the PV installed capacity in Europe 2050 (IRENA, 2020a). The other sources to estimate the needed PV IC in 2050 are the Energy Watch Group (Ram *et al.*, 2017) and SolarPower Europe (SolarPower Europe and LUT University, 2020). An overview of the sources and their estimates can be found in Table 1.

Table 1: Estimates of installed PV capacities for 2050.

| | Installed PV capacity 2050 [TW] | Comment / Scenario |
|--|------------------------------------|--|
| SolarPower Europe (SolarPower Europe and LUT University, 2020) | 4.7 – 8.8 | 4.7 TW in the Laggard scenario, 7.7 TW in the Moderate scenario and 8.8 TW in the Leadership scenario. |
| IRENA (IRENA, 2020a) | 0.891 | REmap Case |
| Energy Watch Group (Ram et al., 2017) | 1.94 | 100% RES scenario of the Energy |

2.1.4 Electricity consumption data

Electricity consumption data are taken from [Open Power System Data](#) (Wiese et al., 2019). For countries that are missing in Open Power System Data (opsd), the data from the statistical office of the European Union (Eurostat, 2021) is used as a source. Since the data availability per year differs per country, we take the latest fully reported year for each country as current total electricity consumption (range between 2016 and 2019).

Table 2: Overview of all considered countries with their installed PV capacity of 2019 (IRENA, 2020b), their planned installed PV capacity for 2030 from the National Energy and Climate Plans and their mean capacity factors (1985-2016) from Renewables.ninja.

| | Installed PV capacity 2019 [MW] | Planned installed PV capacity 2030 [MW] | Mean PV capacity factor 1985-2016 |
|-------------------------------|------------------------------------|--|--------------------------------------|
| Albania | 3 | 9 | 0.16 |
| Austria | 1'578 | 2'500 | 0.14 |
| Belgium | 4'531 | 15'000 | 0.12 |
| Bosnia and Herzegovina | 18 | 45 | 0.15 |
| Bulgaria | 1'065 | 3'216 | 0.15 |
| Croatia | 69 | 768 | 0.14 |
| Cyprus | 129 | 3'975 | 0.18 |
| Czechia | 2'070 | 3'975 | 0.13 |
| Denmark | 1'079 | 7'842 | 0.11 |
| Estonia | 107 | 415 | 0.11 |
| Finland | 215 | 700 | 0.09 |
| France | 10'562 | 44'000 | 0.14 |
| Germany | 48'960 | 98'000 | 0.12 |
| Greece | 2'763 | 7'700 | 0.16 |
| Hungary | 1'277 | 6'454 | 0.14 |
| Ireland | 36 | 1'250 | 0.11 |
| Italy | 20'900 | 51'200 | 0.15 |
| Latvia | 3 | 9 | 0.11 |
| Lithuania | 103 | 792 | 0.11 |
| Luxembourg | 150 | 1'000 | 0.13 |
| Malta | 154 | 266 | 0.17 |
| Moldova | 4 | 12 | 0.14 |
| Montenegro | 3 | 9 | 0.16 |
| Netherlands | 6'725 | 27'000 | 0.12 |
| Norway | 90 | 265 | 0.10 |
| Poland | 300 | 7'300 | 0.12 |
| Portugal | 828 | 9'000 | 0.17 |
| Republic of North | 26 | 77 | 0.15 |
| Romania | 1'386 | 5'100 | 0.14 |
| Serbia | 10 | 25 | 0.15 |
| Slovakia | 472 | 1'200 | 0.13 |
| Slovenia | 222 | 1'650 | 0.14 |
| Spain | 8'761 | 39'200 | 0.17 |
| Sweden | 644 | 2'650 | 0.10 |
| Switzerland | 2'524 | 4'400 | 0.15 |
| United Kingdom | 13'398 | 39'478 | 0.11 |
| Sum | 131'165 | 386'481 | |

2.2 Method

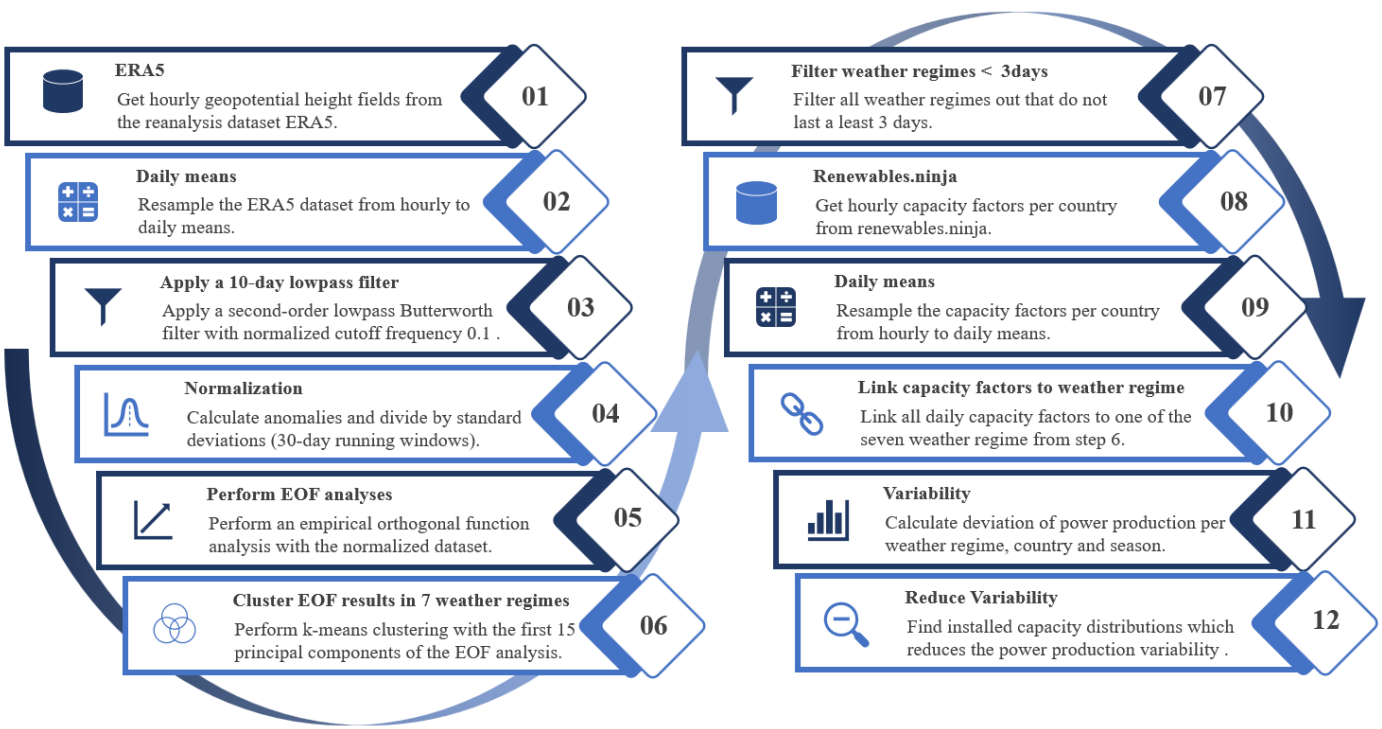


Figure 3: Overview of the approach to derive the weather regimes, link the country-specific capacity factors, and find a distribution that reduce the PV power production variability.

2.2.1 Weather regime classification

As the first step, we resample the hourly 500 hPa geopotential height fields from ERA5 by calculating daily means for each 2D grid point (Figure 3, step 2). Afterwards, a 10-day lowpass filter is applied because weather regimes are a low-frequency phenomenon and typically last several days. We apply the 10-day lowpass filter with the python package [scipy.signal.butter](#) (Virtanen et al., 2020), which has implemented the Butterworth filter design. A filter order of two and a critical frequency of 0.1 (10-days) are used as the filter parameters (Figure 3, step 3). The lowpass filtered daily means (z_d) are used to calculate standardized anomalies (z_{norm_d}) which are the input data for the EOF analysis (see below):

$$z_{norm_d} = \frac{z_d - z_{d,mean}}{z_{d,std}} \quad \text{Eq. 2}$$

where $z_{d,mean}$ are the climatology of the 500 hPa geopotential height daily means with a running window of 30 days, and $z_{d,std}$ are the standard deviations of the 500 hPa geopotential height daily means with a running window of 30 days. The running window is defined as the respective day acting as the window's centre. For instance, to derive the reference climatology for the 15th of January, the mean from the first to the 30th of January is calculated for every year and grid point. This results in 41 means per grid point since our dataset covers 41 years. These 41 means per grid point are retaken to calculate a mean so that we finally have one

reference climatology for the 15th of January for every grid point. This is done analogously for every day of the year, which yields 366 separate reference climatology and standard deviations per grid point.

Since the standardized anomalies include normalizing with the standard deviation, the amplitude in the anomaly caused by the seasonal cycle is removed before the weather regime classification. The removal of the anomaly caused by the seasonal cycle clears the way to define the WR year-round. Our choice to use a 30-day running window for the reference climatology and standard deviation calculations differs from other studies. Often, investigations are made for weather regimes in winter where a correction for the seasonality is not needed. Others are using 90-day averaging periods (Grams *et al.*, 2017). Still, since our interest focuses on multiday timescale, this is rather long and increases the probability that the impact of the seasonal cycle signal is relatively high.

For the weather regime classification (Figure 3, step 5 and 6), we use empirical orthogonal function analysis and k-means clustering (Cassou, 2008; Michelangeli *et al.*, 1995). An EOF analysis decomposes a dataset into statistically orthogonal modes and corresponding time-series that describe the data's variability. For meteorological datasets, a few modes are often sufficient to explain a large fraction of the data's total variability, which helps to assess the key patterns of the variability and further analyse them. We perform the EOF analysis on the standardized anomalies with the [eof](#) python package by Dawson (2016). The EOF analysis is performed with the square root of the cosine of latitude as weights to consider the change in grid box size with latitude.

The resulting first 16 principal components of our EOF analyses, which explain ~90% of the variance, are used to cluster the data into weather regimes (Figure 3, step 6). We use the clustering method k-means implemented in the python package [sklearn.cluster](#) by Pedregosa *et al.* (2011). Generally, clustering techniques are used to group data with similar characteristics by minimizing the clusters' variance. The difficulty lies in the definition of the number of clusters. For the Euro-Atlantic region, four clusters commonly are used to define the weather regimes (Cassou, 2008; Michelangeli *et al.*, 1995; van der Wiel *et al.*, 2019). The four weather regimes received with this approach are the negative and positive phase of the North Atlantic Oscillation, the Scandinavia high and the Atlantic ridge. Most of these studies focus only on wintertime weather regime classification. According to Grams *et al.* (2017), the optimal number of clusters to define weather regime year-round is seven. We also use seven clusters which enable direct comparison/combination with the study by Grams *et al.* (2017). Furthermore, we exclude all days where a weather regime does not last at least three days and assign these days to a separate weather regime hereafter called "no-regime" (Figure 3, step 7). This is done by checking the time-series after the clustering and finding all days where a weather regime does not prevail for at least three subsequent days and assign it to "no-regime".

To summarise, we use EOF analysis to decompose our dataset (standardized anomalies of geopotential height) and find the modes which explain the largest fraction of the variability. Afterwards, the

EOF analysis results are used to cluster the data, which allows deriving an assignment for each day of the ERA5 dataset to one of seven weather regimes.

2.2.2 Capacity factors and PV power production variability

As the first step in deriving capacity factors and PV power production variability, the CF dataset is resampled to daily means (Figure 3, step 9). Since the CFs are highly influenced by the seasonal cycle, they are analysed separately for each season. The seasons are defined with the months December, January, February (DJF) for winter - March, April, May (MAM) for spring - June, July, August (JJA) for summer and September, October, November (SON) for autumn. With the weather regime classification, the capacity factor can be linked to the different weather regimes (Figure 3, step 10). The linked capacity factors are used to calculate mean capacity factors per weather regime, country, and season ($CF_{wr,country,season}$). The difference between these mean capacity factors per weather regime and the mean capacity factors for the whole season of a country ($CF_{country,season}$) determines whether the weather regime exhibits over- or underproduction relative to the mean (Eq. 3).

$$\Delta CF_{wr,country,season} = CF_{wr,country,season} - CF_{country,season} \quad \text{Eq. 3}$$

Multiplication of capacity factors with installed capacities yields power output (Eq. 1). This can be used to expand Eq. 3, which gives the total deviation of PV power production of Europe per weather regime and season (Figure 3, step 11).

$$\Delta P_{wr,Europe,season} = \sum_{country} (\Delta CF_{wr,country,season} * IC_{country}) \quad \text{Eq. 4}$$

where $IC_{country}$ is the installed PV capacity per country [W].

Eq. 4 is used as an expression for the variability and the basis to achieve the objective of reducing PV power production variability as outlined in the introduction of this study. To illustrate the meaning of the equations, assume that the result of this equation is zero. In that case, the respective weather regime and season's PV power production are equal to the season's mean PV power production. Therefore, the variability is maximally reduced. If the results for every WR and season of Eq. 4 are zero, the PV power production is constant in each season. That would imply that the variability is zero, which massively reduces the challenge to consider the PV power production for power grid balancing purposes.

The consideration of seven weather regimes plus no regime and four seasons implies 32 results of Eq. 4 for the variability. To consolidate these 32 results, we introduce the mean PV power production variability and maximum PV power production variability. The mean PV power production variability is

defined as the sum of the absolute changes in PV power production resulting from the transition from one weather regime to another, weighted with the corresponding frequency of the change:

$$mean_var = \sum_{i=0}^n \sum_{j=0}^n \left(|(\Delta P_{wr_i, Europe, season} - \Delta P_{wr_j, Europe, season})| * f_{i,j} \right) \quad Eq. 5$$

where n is the total number of weather regimes, $\Delta P_{wr_i, Europe, season}$ is the deviation of PV power production from the seasonal mean for a specific weather regime wr_i , $f_{i,j}$ is the frequency of the transition from weather regime i to j. We calculate the frequency by dividing the number of transitions from weather regime i to j per season and the total number of transitions per season.

The maximum PV power production variability is defined as the difference between the weather regime with the highest PV power production ($\Delta P_{wr_{max}, Europe, season}$) and the weather regimes with the lowest PV power production ($\Delta P_{wr_{min}, Europe, season}$) per season:

$$\max_var = \Delta P_{wr_{max}, Europe, season} - \Delta P_{wr_{min}, Europe, season} \quad Eq. 6$$

Total mean and maximum PV power production variability are defined as the average of the obtained results from Eq. 5 and Eq. 6 over the whole season.

2.2.3 Variability reduction with optimized installed PV capacity distribution

To determine an IC distribution aiming to reduce the PV power generation variability, we use Eq. 4 for every country, season, and weather regime in a linear least-square problem with an upper and lower bound on the variables (Figure 3, step 12). This is done with the [scipy.optimize.lsq_linear](#) python package (Virtanen et al., 2020), which solves the following optimization problem:

$$\begin{aligned} & \text{minimize } 0.5 \times ||A\vec{x} - \vec{b}||^2 \\ & \text{subject to } lb \leq x \leq ub \end{aligned} \quad Eq. 7$$

where A is the coefficient matrix, x is the solution found, b is the target vector, lb is the lower bound of the solution x, and ub is the upper bound of the solution x.

The coefficient matrix A is defined with $\Delta CF_{wr, country, season}$ from Eq. 3:

$$A = \begin{pmatrix} \Delta CF_{WR0, AL, winter} & \dots & \Delta CF_{WR0, SK, winter} \\ \vdots & \ddots & \vdots \\ \Delta CF_{WRX, AL, autumn} & \dots & \Delta CF_{WRX, SK, autumn} \end{pmatrix} \quad Eq. 8$$

where the first element of the matrix $\Delta CF_{WR0,AL,winter}$ is the capacity factor anomaly of weather regime 0, in Albania in winter. The columns of A are associated with the 36 different countries considered (Table 2), whereas the eight weather regimes and four seasons translate into the 32 rows of A.

The target vector \vec{b} is set to zero, reducing the variability within one weather regime and season as much as possible and therefore also reducing the variability from one weather regime to another:

$$\vec{b} = [0, \dots, 0] \quad \text{Eq. 9}$$

where \vec{b} has the same length as the number of rows of matrix A.

The result of this method is the vector \vec{x} which contains the IC for each country:

$$\vec{x} = [IC_{AL}, \dots, IC_{SK}] \quad \text{Eq. 10}$$

The method to perform the minimization is the Trust Region Reflective algorithm (Branch et al., 1999). The lower bound is always set to the current (2019) PV IC per country (unless explicitly mentioned in the scenarios below). The upper bound is always set to the roof-top mounted PV potential per country taken from the study by Tröndle et al. (2019).

2.2.4 Scenarios

Besides reducing PV power production variability, we may demand a certain minimum power production on a European scale or a maximum on the installed PV capacity to control associated costs or combinations of the two, or yet other conditions. We analyse four different scenarios, which are shortly summarized in the following table:

Table 3: Overview of the four scenarios to analyse the reduction potential of PV power production variability.

| Scenario | Description |
|----------|--|
| S1 | Retain PV power production in 2030 but reduce PV power production variability. |
| S2 | Retain PV power production in 2050 but reduce PV power production variability. |
| S3 | Retain PV power production but reduce IC (costs) and PV power production variability (2030 S3-1, and 2050 S3-2). |
| S4 | Retain PV power production in 2030 but produce 10% of consumption with PV systems in-land and reduce PV power production variability (S4-1). Extend S4-1 to the year 2050 and to 30% of demand covered with PV systems (S4-2). |

Below we elaborate on the four scenarios described in Table 3. Their constraints are added row/elementwise to the coefficient matrix A (Eq. 8), and the target vector \vec{b} (Eq. 9). The newly added rows and elements act as additional equations within our linear least-square problem, and their residuals are consequently also minimized. But first, we turn again to the associated equations and the question of weighting.

To meet the requirements of the different scenarios described below and get better control over our linear least-square problem, we introduce a weighting vector \vec{w} :

$$\vec{w} = [w_0, \dots, w_x] \quad \text{Eq. 11}$$

where the elements of the vector \vec{w} are the weightings for each of our equations defined with the coefficient matrix A and the target vector \vec{b} . The weighting vector is also useful to consider the various orders of magnitudes of our equations. I.e., the first 32 rows are of the same order of magnitude because they all describe the PV power production variability. But this is not the case if we introduce an equation/row which constrains our system to a minimum total European PV power production. Additionally, it must be considered that the method used to solve the linear least-square problem minimizes the sum of the residuals of the equations. Since our first 32 equations are all about variability, they are already relatively highly weighted compared to one equation we add with the same order of magnitude. With the introduced weighting vector, it is possible to counteract and give more weight to the one added equation if necessary.

To apply the weighting vector, the square root of its elements is taken as elements of a diagonal matrix and is multiplied with the coefficient matrix A and the target vector \vec{b} , before the optimization problem is solved (Eq. 12 and Eq. 13).

$$A_w = A \cdot \begin{pmatrix} \sqrt{w_0} & \cdots & 0 \\ \vdots & \ddots & \vdots \\ 0 & \cdots & \sqrt{w_x} \end{pmatrix} \quad \text{Eq. 12}$$

$$\vec{b}_w = \vec{b} \cdot \begin{pmatrix} \sqrt{w_0} & \cdots & 0 \\ \vdots & \ddots & \vdots \\ 0 & \cdots & \sqrt{w_x} \end{pmatrix} \quad \text{Eq. 13}$$

In the following, we introduce the already mentioned scenarios for capacity allocation in the future in greater detail.

2.2.4.1 Scenario 1 (S1) – Retain PV power production in 2030, but reduce variability

The objective of scenario S1 is to minimize the PV power production variability while the total power production with PV systems in Europe must remain the same (+/- 1 GW) as estimated with the NECPs for 2030. This gives a direct comparison of the variability estimated with the plans of the countries in Europe for 2030 to the variability estimated with an optimal distribution of installed PV capacities that produces the same amount of electricity. It shows the overall potential of the PV power production variability reduction with an optimized IC distribution.

To implement S1, one row and element are added to the coefficient matrix A and the target vector \vec{b} , respectively. PV power production is calculated by multiplying IC and CF (Eq. 1). Therefore, we add all the mean CF per country as a row to the coefficient matrix A. The total PV power production, estimated with the NECPs for 2030, is added to the target \vec{b} .

$$A_{S1} = \begin{pmatrix} \cdots & \cdots & \cdots \\ \vdots & \ddots & \vdots \\ CF_{AL} & \dots & CF_{SK} \end{pmatrix} \quad \text{Eq. 14}$$

where A_{S1} is the coefficient matrix for S1 (expansion of Eq. 8) and CF_{AL} and CF_{SK} are the mean capacity factors for Albania and Slovakia, which are alphabetically the first and last considered countries.

$$\overrightarrow{b_S1} = [\dots, tot_{production_2030}] \quad \text{Eq. 15}$$

where b_S1 is the target vector for S1 (expansion of Eq. 9), and $tot_{production_2030}$ is the total PV power production estimated with the planned IC for 2030.

The weighting vector for S1 is chosen such that the equation considering the total PV power production gets 10times as much weight as each individual equation considering variability.

2.2.4.2 Scenario 2 (S2) – Retain PV power production in 2050, but reduce variability

In scenario S2, estimates of installed PV capacities for 2050 are taken to calculate the corresponding PV power production and use it as an additional equation in our linear least-square problem. Like S1, it is achieved by adding a row with all the mean CF per country to the coefficient matrix A and the total PV power production estimates for 2050 as an element to the target vector \vec{b} .

S2 is calculated three times, first with the lowest value estimated by IRENA with 0.891 TW (S2-1), second with the intermediate estimation by the Energy Watch Group of 1.94 TW (S2-2) and third with the highest estimation by SolarPower Europe in their Leadership scenario with 8.8 TW (Table 1, page 8.). The weighting vector for S2 is chosen such that the equation considering the total PV power production gets 10times as much weight as each individual equation considering variability.

To put the results in context, we also calculate the variability with the same amount of installed PV capacity but percentual equally distributed to the countries as it was in the year 2019.

2.2.4.3 Scenario 3 (S3) – Cost and variability minimization

In addition to the PV power production variability reduction (S1, S2), S3 focuses on minimizing the costs. This is done by minimizing the amount of installed PV capacity with the constraint that they must produce the same amount of electricity as estimated with the installed PV capacity planned in the NECPs for 2030 (S3-1). We perform the same analysis in a second run, but with the estimate for 2050 of 1.94 TW installed PV capacity by the Energy Watch Group (S3-2). The constraint for the PV power production is added in a similar way as in S1. The consideration of minimal installed PV capacities is achieved by adding a row with ones to the coefficient matrix A and zero as an element to the target vector \vec{b} . This equation sets the total installed PV capacity to zero and therefore, every added installed PV capacity per country acts as residual of this equation. This residual is minimized by the linear least-square optimization together with the residuals for the variability and the PV power production.

The weighting vector for S3 is chosen such that the equation considering the total PV power production gets 10times as much weight as each individual equation considering variability and 100times as much weight as the equation considering total IC.

2.2.4.4 Scenario 4 (S4) – Coverage of country-specific electricity consumption

Scenario 4 has two sub scenarios. The objective of scenario S4-1 is to minimize the PV power production variability, while each country must generate 10% of its electricity consumption with PV systems itself in the year 2030. The latest (between 2016 and 2019) available yearly electricity consumption data (section 2.1.4) is taken as a source for this purpose. Projections of electricity consumption for 2030 are neglected because the focus is on what happens with the variability if we enforce a flatter distribution of the installed PV capacities rather than on actual percentual coverages of the consumption per country. S4-1 is constructed like S1, but instead of the currently installed PV capacities for each country as lower bound, S4 uses 10% of the yearly consumption per country divided by the CF per country as lower bound.

$$lb_{country} = 10\% \times \frac{load_{country}}{CF_{country} * 365d * 24 \frac{h}{d}} \quad \text{Eq. 16}$$

where $lb_{country}$ is the lower bound for the installed PV capacity per country [W], $load_{country}$ is the yearly electricity consumption per country [Wh], and $CF_{country}$ is the capacity factor per country [unitless].

To further analyse S4, it is run a second time for 2050 with the estimates of 1.94 TW installed PV capacity by the Energy Watch Group (S4-2). The same consumption data as in S4-1 are used, but the electricity consumption coverage with PV systems is set to 30%.

3. Results

Chapter 3 gives an overview of the obtained results. First, it describes the derived weather regimes and the linked CF anomalies per country and season. Second, the scenarios' results and their installed PV capacity distributions and variability are presented. Overall, we find that both existing and planned, installed PV capacity distributions lead to significant variability in PV power production depending on the weather regime. We present alternative spatial distributions of installed PV capacity that substantially reduce this variability while respecting selected additional constraints. The latter include total PV power production and constraints like cost minimization (least possible installed PV capacity) or local PV power production targets.

3.1 Weather regimes and their linked capacity factor anomalies

Figure 4 gives an overview of the derived weather regimes and their relation to the two most important input variables for GSEE, namely the surface solar radiation and the 2m temperature. In Figure 4a) the weather regimes are presented as standardized geopotential height anomalies (Eq. 2) and their frequency of occurrence. Surface solar radiation and 2m temperature are also presented as standardized anomalies in Figure 4b) and Figure 4c), respectively. A standardized anomaly of 0.5 means that the difference of the weather regime average and the climatological 30-day running mean amounts to 50% of the 30-day climatological standard deviation. From Figure 4, it can already be taken that both weather variables show distinct, WR-specific patterns, which are discussed in more detail below. An overview of the WR frequency can be found in Figure 6 and Appendix Table 8, illustrating that some WRs preferentially occur in some seasons. For instance, WR0, WR2, WR3, and WR5 are the dominating weather regimes in winter, whereas WR1, WR3, WR4, and WR5 dominate in summer. The relation between the weather regime number and the ordinary names, which are often used in literature, can be found in Table 4.

The link between the weather regimes and the derived capacity factor anomalies is shown in Figure 5. The first row of Figure 5 shows the seven weather regimes plus no regimes again. Beneath the weather regimes, in the same column, the corresponding country-specific capacity factor anomalies can be found. The different seasons are shown separately. The capacity factor anomalies are calculated as the related seasonal mean difference. There are several reasons to treat the CF anomalies separately per season. One of them is the different seasonal cycle of wind (highest in winter) and PV power production (highest in summer) and their combination possibilities to balance the power grid. Another reason is the difference in electricity consumption per season and, combined with the production, its risk for the energy system. Again, it is obvious from just looking at the figure that WRs play a decisive role in country-specific capacity factors. A detailed discussion is given below.

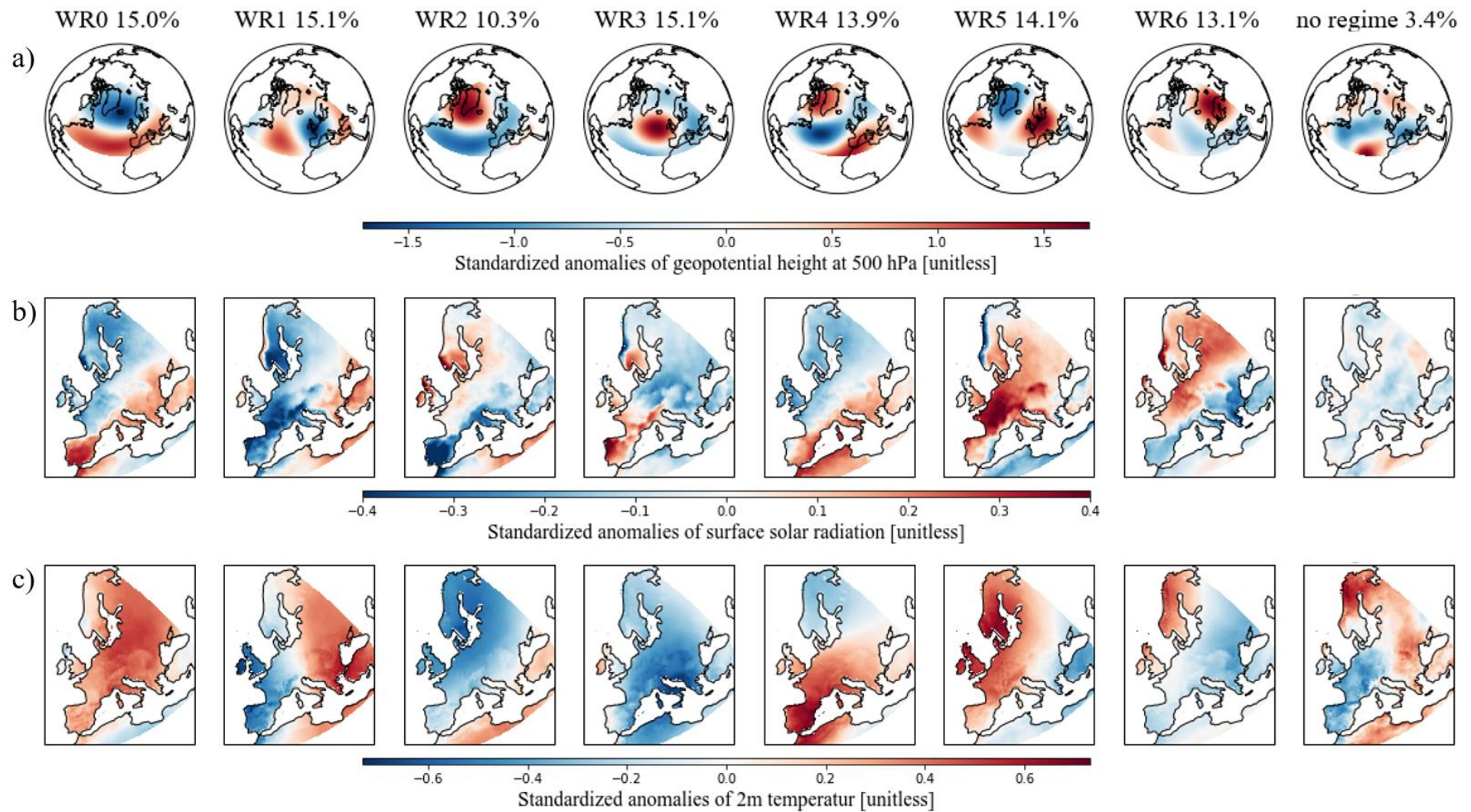


Figure 4: Different variables of the derived seven weather regimes and “no regime” plus their frequency of occurrence. a) Standardized anomaly fields of geopotential height at 500 hPa. b) Standardized anomaly fields of surface solar radiation. c) Standardized anomaly fields of 2m temperature.

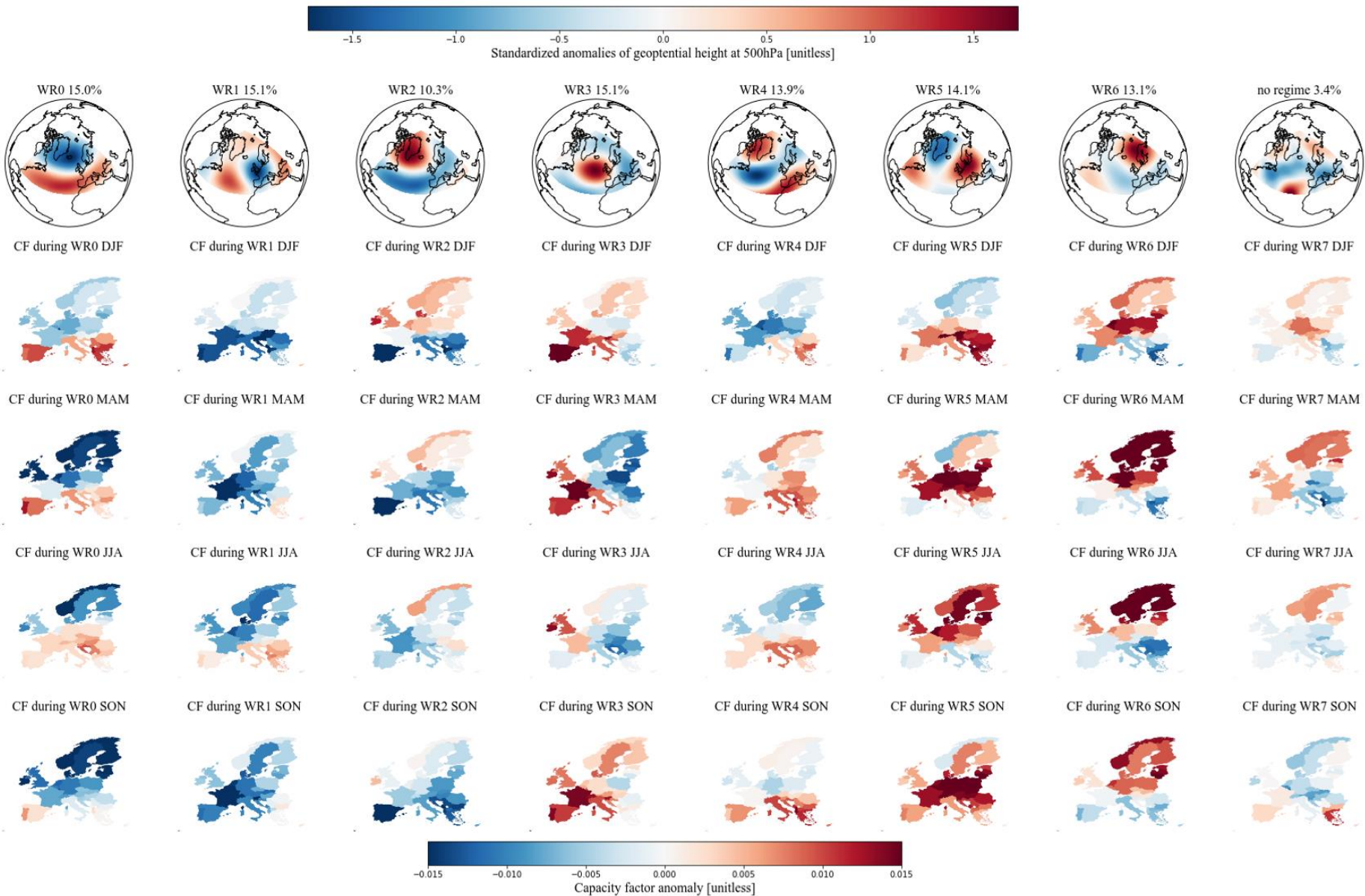


Figure 5: Link between the derived seven weather regimes and the capacity factor anomalies per country and season. The first row shows standardized anomaly fields of geopotential height at 500 hPa for each weather regime. The linked capacity factor anomalies per country are shown separately for each season and are calculated as difference to the corresponding seasonal mean: winter (DJF), spring (MAM), summer (JJA) and autumn (SON).

Table 4: Relation between weather regime numbers and common weather regime names.

| | |
|------------|---|
| WR0 | The positive phase of the North Atlantic Oscillation (NAO+) |
| WR1 | European trough |
| WR2 | The negative phase of the North Atlantic Oscillation (NAO-) |
| WR3 | Atlantic ridge |
| WR4 | Atlantic trough |
| WR5 | European blocking |
| WR6 | Scandinavian blocking |

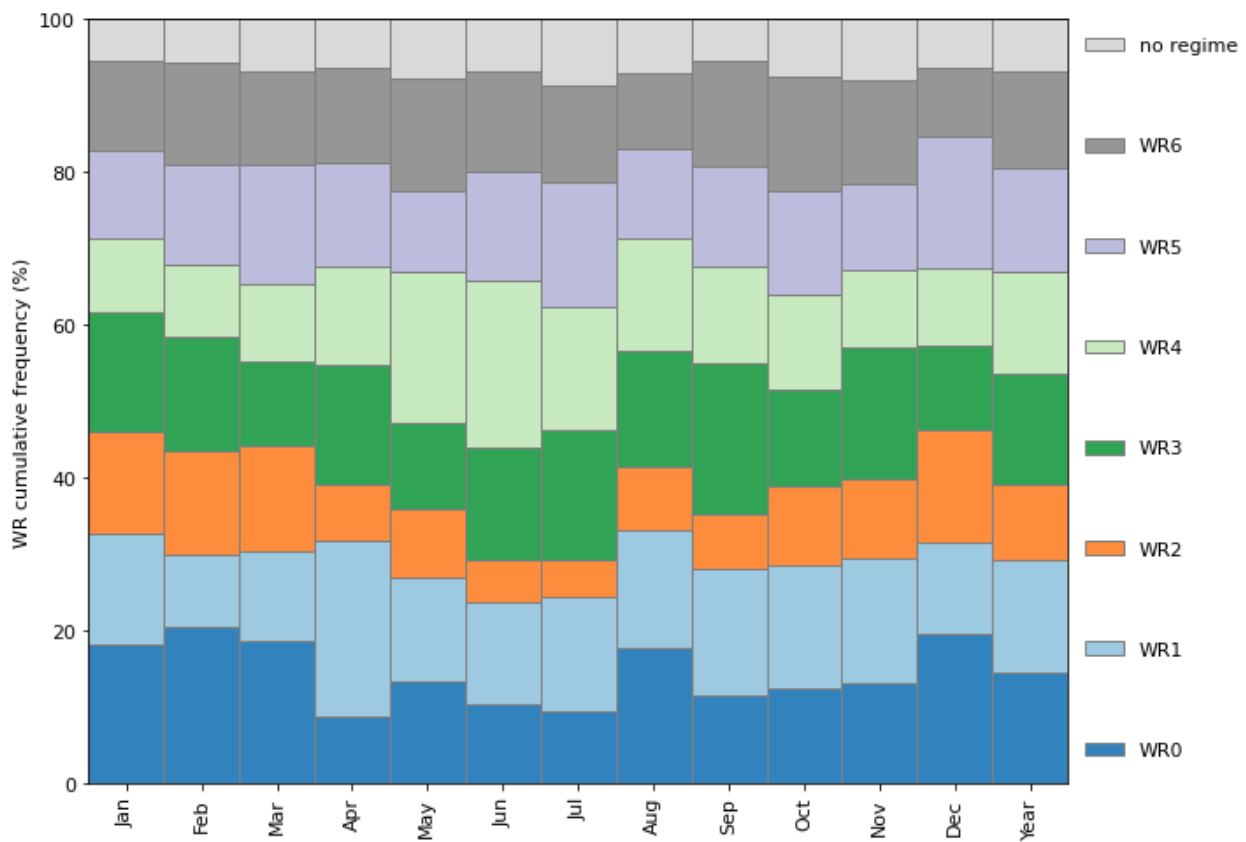


Figure 6: Cumulative frequency of the seven weather regimes (WR) and no regime.

3.1.1 Weather regime 0 - NAO+

A negative geopotential height anomaly (cyclone) over the Northern part of the Atlantic and a positive geopotential height anomaly (anticyclone) over the Atlantic/Mediterranean sector is the characterizing feature of the positive phase of the NAO. During these conditions, the Atlantic storm tracks are displaced North-eastward, and the zonal flow is enhanced. This increases the strength of the westerlies and brings maritime air (warm and moist) to Central and Northern Europe (Hurrell et al., 2003; Rogers, 1997; Wallace & Hobbs, 2006). Consequently, the storm track activity over Northern Europe is enhanced, leading to a larger cloud cover fraction and less available surface solar radiation. Studies by Pozo-Vázquez *et al.* (2004; 2011) have shown that the NAO index is negatively correlated with the surface solar radiation in Northern Europe and positively correlated with surface solar radiation in southern Europe. Our results agree with these studies with negative surface solar radiation anomalies in Northern Europe, positive surface solar radiation in Southern Europe and positive temperature anomalies almost all over Europe (Figure 4b) and c), the first column).

During the positive phase of the NAO, the CF anomalies also exhibit a clear North to South discrepancy. Northern Europe shows negative CF anomalies, whereas positive CF anomalies dominate southern Europe. This is in line with the surface solar radiation described above, but the pattern changes throughout the season. In spring, the results show a significant and clear difference between Southern and Northern Europe. But in autumn, only the Iberian Peninsula and a few countries in South-eastern Europe exhibit positive CF anomalies.

3.1.2 Weather regime 1 - European trough

WR1 is characterized by a meridional dipole of a positive and negative geopotential height anomaly in the Atlantic and Western Europe. The cyclone located over Western Europe brings relatively warm air from the South to South-eastern Europe, and higher temperature above average can be observed (Figure 4c), WR1). Surface solar radiation anomalies are also enhanced in South-eastern Europe but are not as pronounced. Western Europe, where the cyclone is located, shows negative temperature and surface solar radiation anomalies except the Northern part of the British Isles and the Western coast of Norway, which lies on the northern edge of the cyclone.

The CF anomalies during the European trough are mostly negative, which agrees with the surface solar radiation's overall pattern. It does not fit in winter, where Southern and South-eastern Europe exhibit an even larger negative impact than Northern Europe. In contrast, the surface solar radiation for the whole year is positive in this region. Interestingly, this weakens in spring and even turns into positive CF anomalies in summer, which is more in line with our surface solar radiation anomalies presented year-round. This may be attributable to WR1 being less frequent in winter than summer and spring (Figure 6).

3.1.3 Weather regime 2 – NAO-

Contrary geopotential height anomaly fields relative to the positive phase of the NAO can be found in the negative phase of the NAO (WR2). It is characterized by a negative geopotential height anomaly over the Atlantic/Mediterranean sector and a positive geopotential height anomaly over Greenland. This also results in contrary surface weather variables relative to the positive phase of the NAO. It exhibits higher surface solar radiation compared to the climatological average in Northern Europe and lower surface solar radiation in Southern Europe. The temperature anomalies are negative all over Europe.

The contrary pattern to the positive NAO is also reflected in the CF anomalies with positive values in Northern Europe and negative values in the South. But we can see here that this discrepancy between North and South is evident in winter and spring but weakens in summer and autumn, where more negative CF anomalies are present in Northern regions. Again, the cause may lie in the more frequent occurrence of WR2 during winter times (Figure 6).

3.1.4 Weather regime 3 - Atlantic ridge

The Atlantic ridge (WR3) exhibits a strong positive geopotential height anomaly (anticyclone) over the Atlantic. Enhanced surface solar radiation anomalies can be seen in Western Europe, mainly over the Iberian Peninsula and Southern Scandinavia. These regions are located at the western edge of the anticyclone. This could explain the enhanced surface solar radiation because of the relation between anticyclones and descending air and clear sky conditions. Eastern Europe, which is already outside of the anticyclone region, shows negative surface solar radiation. The anticyclone brings relatively cold air from the North to Europe. Therefore, one can observe negative temperature anomalies all over Europe except the Western coast of the Iberian Peninsula and the British Isles.

The East-West gradient is also visible in the CF anomalies, with positive anomalies in the West and negative anomalies in the East. The seasonal differences are substantial: In spring, one can observe a strong East-West gradient. In winter and autumn, one can still see a discrepancy between East and West, but the anomalies are less pronounced and generally more often positive. The opposite is the case during summer, where one can see more frequent but less enhanced negative anomalies, with a persisting East-West gradient.

3.1.5 Weather regime 4 - Atlantic trough

WR4, the Atlantic trough, shows a meridional dipole pattern of the geopotential height anomaly reversed to WR, but the cyclone and anticyclone are more elongated in the meridional direction. The negative anomaly is located over the Atlantic and Northern Europe, and the positive anomaly is located over the Mediterranean sector. It can be best compared with the Atlantic trough weather regime (Grams et al., 2017), but the positive geopotential height anomaly over South-eastern Europe does not fit well to this association. WR4 exhibits positive temperature anomalies over Southern and Central Europe in the region of the positive geopotential height anomaly and slightly negative temperature anomalies over Scandinavia.

The surface solar radiation anomalies show a clear gradient from South-eastern to North-western Europe. Positive values are located over the Mediterranean region, and negative values anomalies over Scandinavia and the British Isles.

The CF anomalies of the countries in the Mediterranean region resemble the surface solar radiation anomalies and show mostly slightly positive values. In Northern Europe, the difference between seasons is more pronounced. In winter and summer, they are negative, but in autumn and spring, more Northern countries exhibit positive CF anomalies.

3.1.6 Weather regime 5 - European blocking

The blocking situation in WR5 is characterized by a positive geopotential height anomaly (anticyclone) over Central Europe. This is associated with descending air which brings clear skies over Central Europe, and therefore enhanced surface solar radiation anomalies can be observed in Figure 4b, WR5. These anomalies are less pronounced in the Scandinavian region and Eastern Spain or even negative because these regions are situated on the edge of the anticyclone. The temperatures are also increased, especially in North-Western Europe, which is affected by the advection of warm air from the South.

With clear sky conditions, the CF are also higher than usual. Greatly increased CF anomalies can be observed, especially in central Europe. In winter, the CF anomalies are only negative for Scandinavia and the British Isles. Towards summer, these change to positive CF anomalies, whereas it changes to negative CF anomalies for countries in Southern Europe.

3.1.7 Weather regime 6 - Scandinavian blocking

Like the European blocking, the positive geopotential height anomaly (anticyclone) over Scandinavia relates to descending air, clear sky conditions and enhanced surface solar radiation (Figure 4b, WR6). Since the anticyclone is now located more to the North, Southern countries exhibit less surface solar radiation than normal. The positive temperature anomalies have also shifted Northwards to the Scandinavian region. The anticyclone brings relatively cold air from the North to South-eastern Europe, where a negative temperature anomaly can be observed (Figure 4c), WR6).

The CF anomalies show significantly increased values over Northern Europe throughout the year, whereas the CF anomalies in Southern Europe are lower than average.

3.1.8 No regime

The mean geopotential height field of all days assigned to no regime (weather regimes that last less than three days) tends to show slightly negative values over Central Europe and Northern Atlantic. Slightly positive geopotential height anomalies can be observed in Northern Scandinavia. The anomalies are not very pronounced, which we could expect because it is the average of different weather regimes. Also, surface solar radiation is not very pronounced but slightly negative. The 2m temperature shows similar

distribution as the geopotential height anomaly with positive values over Northern-eastern Europe and negative values in South-western Europe.

The CF anomalies show slightly positive values in Northern Europe and slightly negative values in Southern Europe in winter, spring, and summer. It changes in autumn, and Northern Europe has mostly slightly negative CF anomalies, where Southern Europe shows more positive values.

The frequency implies that only 3.4% of all analysed days are not linked to a weather regime. The low frequency might be explained because of the applied 10-day lowpass filter (Figure 3, step 3). The filter already smooths the data before the weather regime classification and reduces significant changes in short time intervals.

3.2 Installed capacity distributions and their variability

Having examined the different WRs in detail in section 3.1, we now turn to the question of WR-associated variability in PV power production and how this variability may be reduced by the spatial distribution of installed PV capacity. To this end, we hereafter present the results of the four scenarios with their IC distributions and PV power production variability. To put the results into context, they are always shown together with the IC distributions and variability of the year 2019 (Figure 7, first panel), with the IC distribution and variability estimated for 2030 (Figure 7, second panel) or the IC distribution and variability estimated for 2050 (Figure 12, first panel).

The total IC in Europe in 2019 was 131.2 GW (IRENA, 2020b). Its distribution is presented in the first plot of Figure 7. Most of the capacity is installed in Western Europe, with Germany as the leading country (see also Table 2). The mean PV power production, estimated with the IC and the capacity factors per country, amounts to 17.5 GW (153 TWh for the whole year 2019). The mean variability, which is the average change of PV power production when the weather regime shifts from one to another, amounts to 0.9 GW (1 GW is roughly the rated capacity of one nuclear power plant). This is about 5.1% of the total mean production. The maximum variability, which is defined here as the difference from the weather regime with the highest PV power production to the weather regime with the lowest PV power production per season, amounts to 3.0 GW. This corresponds to a change in PV power production of 17.1%.

The planned total IC of 2030 is 386.5 GW (NECPs), which is about three times as much as in 2019. Most of the installed capacity is still located in Western Europe (Figure 7, second plot). The mean estimated PV power production increases to 52.3 GW. The mean and maximum variability also roughly triple compared to the year 2019 to 2.7 GW and 8.5 GW, respectively, which is 5.2% and 16.3% of the mean PV power production. A detailed overview of the variability can be found in Figure 10 and Figure 11. Figure 10 shows the deviation (from the seasonal mean) of PV power production per weather regime and season, and Figure 11 present a consolidated (overall weather regimes) view per season.

3.2.1 Scenario 1 – Retain PV power production in 2030, but reduce variability

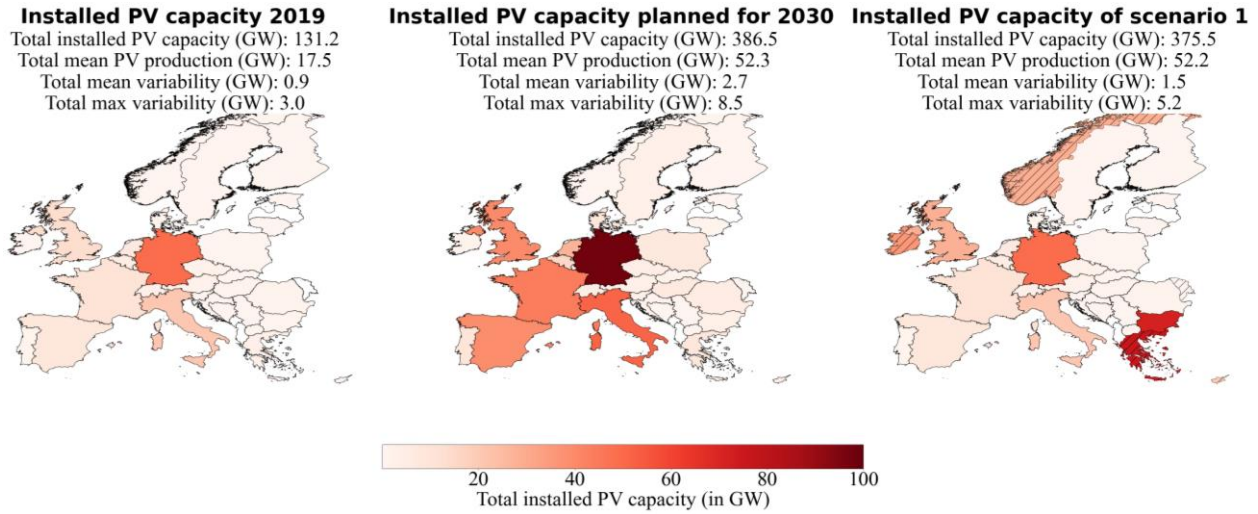


Figure 7: Current (2019), planned for 2030 (NECPs) and resulting from scenario 1 (S1) installed PV capacity distributions. S1 minimized the variability of PV power production with the constraint that the PV power production must be equal to the PV power production estimated for 2030 (NECPs). Hatched countries indicate that the upper bound (potential for roof-top mounted PV systems) is reached.

The IC distribution derived under the conditions of S1 is shown in the third plot of Figure 7. The total mean PV power production is almost the same as the one estimated with NECPs for 2030 (0.1 GW difference), which was the constraint for this scenario. The mean variability could be reduced from 2.7 GW to 1.5 GW, and the maximum variability could be reduced from 8.5 GW to 5.2 GW. This refers to a percentual reduction from 5.2% to 2.9% for the mean variability and from 16.3% to 10.0% for the maximum variability. The reduction of the variabilities, while keeping the PV power production constant, could be achieved with overall less total installed PV capacity of 375.5 GW (compared to 386.5 GW planned for 2030). An overview of the results can also be found in Table 5, page 37.

Figure 8 shows in which countries the additional (difference between 2030 and 2019) installed PV capacities are distributed according to the plans from NECPs (left) and as obtained with our approach to reduce the PV power production variability (right). In contrast to what is planned by NECPs, the method chosen to reduce the PV power production variability favours countries in South-eastern and North-western Europe. Hatching indicates countries where the installed PV capacity has reached the upper bound of the linear least-squares problem, defined as the potential for roof-top mounted PV systems (Tröndle et al., 2019).

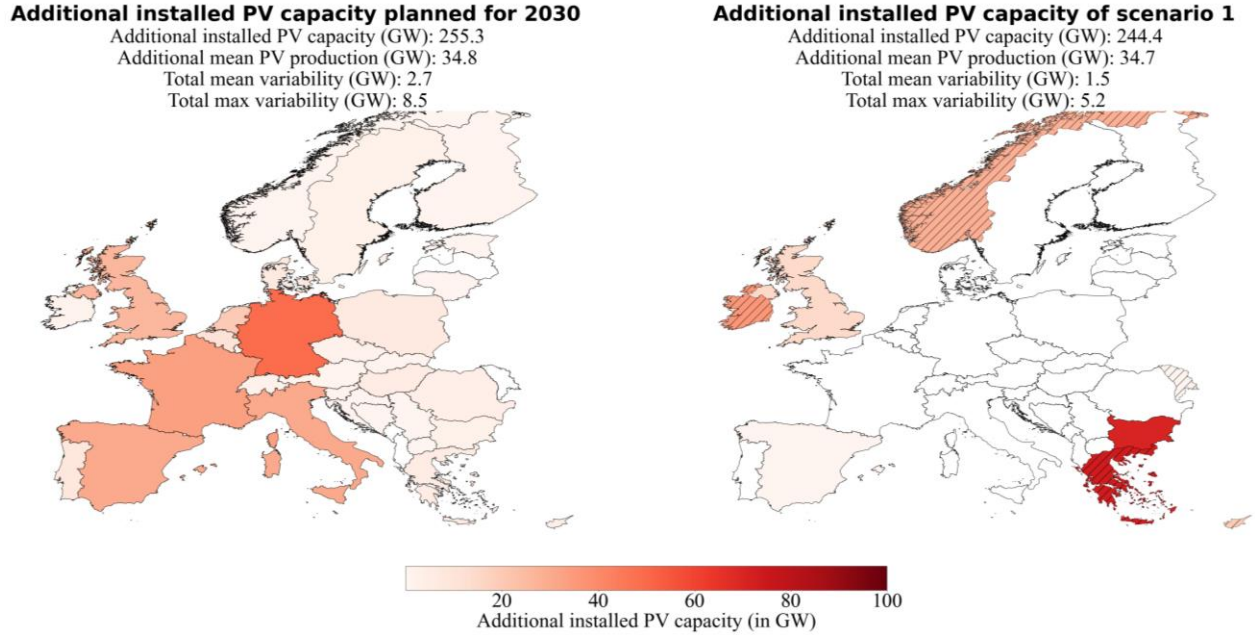


Figure 8: Additional installed PV capacities planned for 2030 (NECPs) and of scenario 1 (S1). S1 minimized the variability of PV power production with the constraint that the PV power production must be equal to the PV power production estimated for 2030 (NECPs). Hatched countries indicate that the upper bound (potential for roof-top mounted PV systems) is reached.

Since the method favours countries on the South-eastern and North-western edge of Europe, it is interesting to see which countries are the next favourites if no additional PV systems can be placed in an already considered country. Therefore, we analysed what happens when setting the upper bound of already considered countries to their current (2019) installed PV capacity. With this approach, no PV systems will be placed in this country, and one can see which country is the next favourite and how much this increases variability. This is done one after the other, first for the countries in South-eastern Europe (Greece, Bulgaria, Romania-Serbia, and Italy) and afterwards for the countries in North-western Europe (United Kingdom, Norway, Ireland, and Finland). The results can be found in Figure 9. White hatching denotes countries where no additional placement of PV systems was allowed. As soon as the upper bound of a South-eastern country is hit, the optimization starts to place the installed capacity to an adjacent country until the point is reached where variability is better reduced by adding the installed PV capacity to countries more to the West (Italy and Spain). The same was done for countries in North-west where the method starts to place the installed PV capacity more to the East (Finland and Denmark). It indicates that suppressing a South-eastern/North-Western distribution makes a South-western/North-eastern distribution the best solution to reduce the variability.

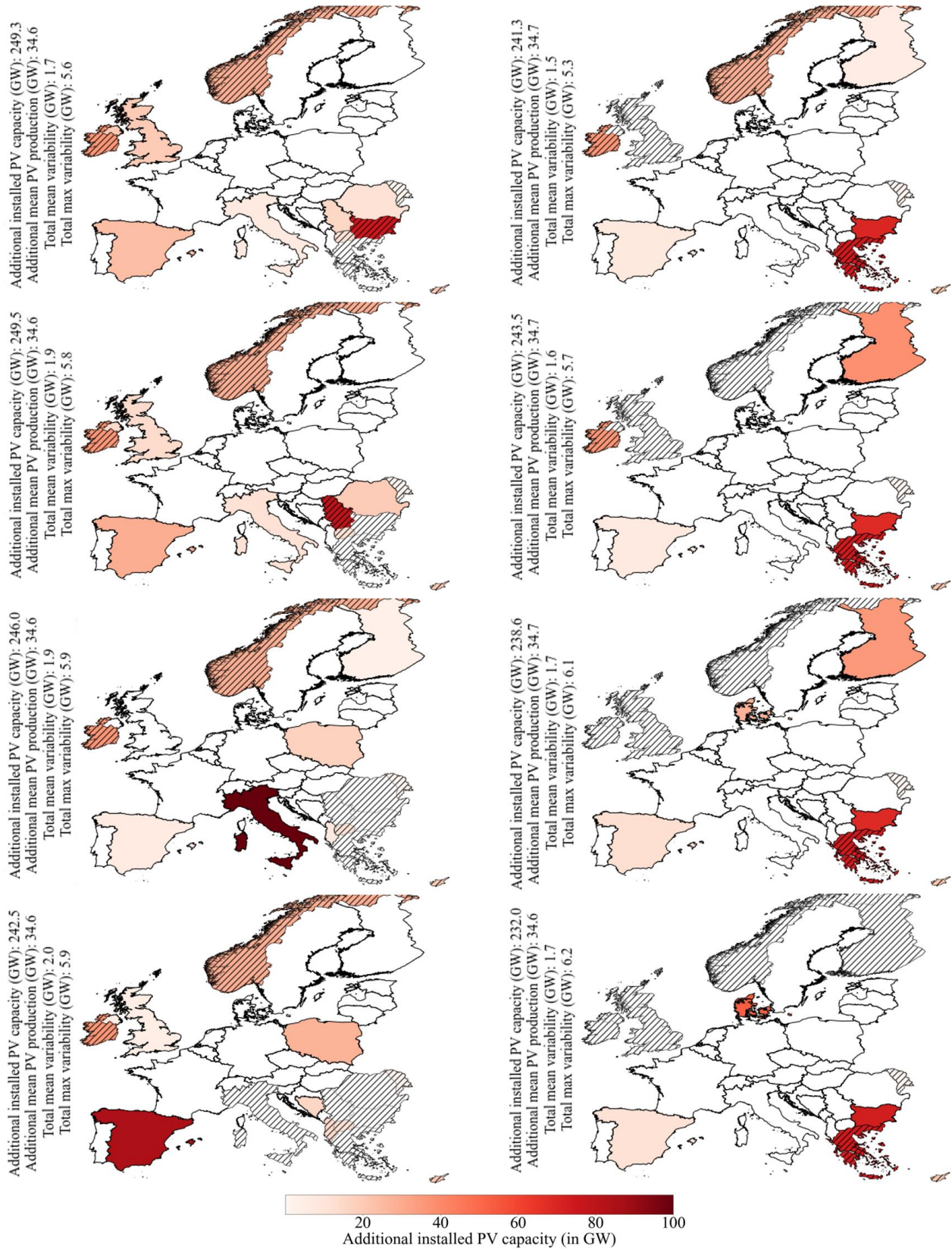


Figure 9: Additional installed PV capacities of modified scenario 1 (S1). The upper bound of some countries (hatched, white) are set to their current installed PV capacity. No additional PV systems will be placed in this country. This is done one after the other, first for the South-eastern countries (upper-left to lower-left panel): Greece, Bulgaria, Romania-Serbia, and Italy. Afterwards for the North-western countries (upper-right to lower-right panel): the United Kingdom, Norway, Ireland and Finland. Hatched colored countries indicate that the upper bound (potential for roof-top mounted PV systems) is reached.

A detailed impression of the over- and underproduction for every weather regime and season compared to their seasonal mean is shown in Figure 10. The IC distribution for scenario S1 reduces the deviation of PV power production from the seasonal mean in 25 of 32 cases (pairs of four season / eight WRs). It also shows that changes from under- to overproduction in weather regimes are possible with different distributions and vice versa.

The consolidated view of the variability (Figure 11) clarifies that the variability tends to be higher in mid-season (spring and autumn). The maximum variability (black markers) is higher in mid-season, with the peak in autumn for all three distributions. Figure 11 also shows that the distribution of S1 reduces the mean and maximum variability in every season and in total.

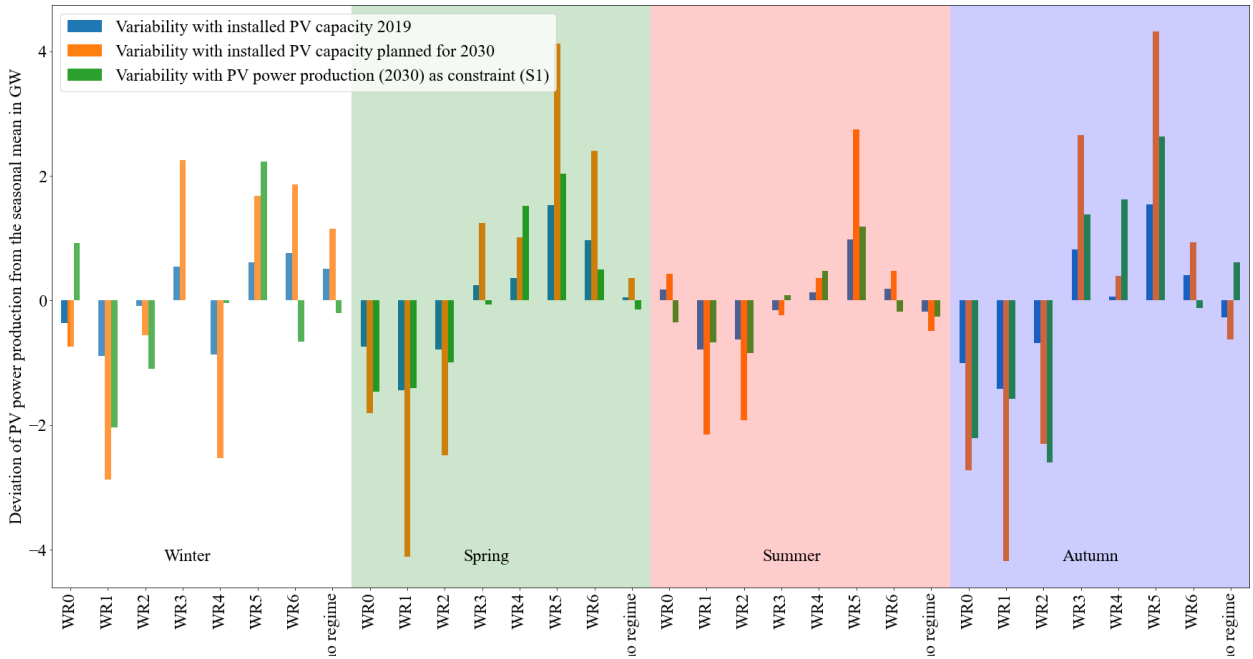


Figure 10: Deviation of the PV power production from the seasonal mean per weather regime and season. In blue the variability for the current situation (2019), in orange the estimated variability with the planned installed capacities for 2030 (NECPs) and in green the estimated variability with the installed capacity distribution for scenario 1.

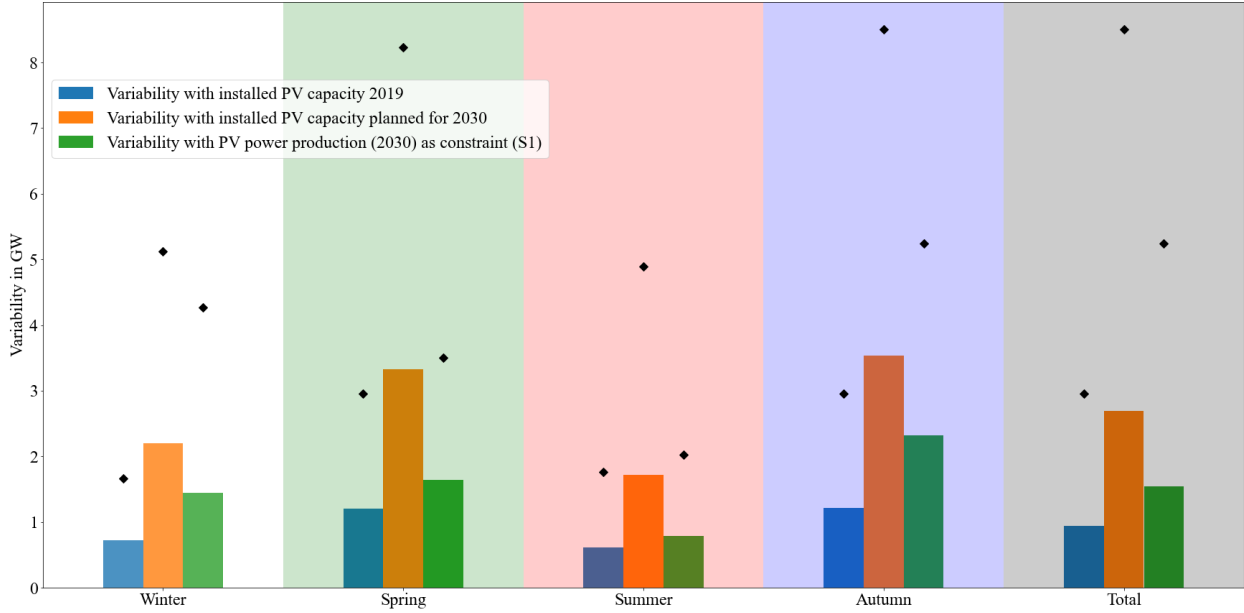


Figure 11: Mean (bars) and maximum (black markers) consolidated (over all weather regimes) variability per season and overall (total). In blue the variability for the current situation (2019), in orange the estimated variability with the planned installed capacities for 2030 (NECPs) and in green the estimated variability with the installed capacity distribution for scenario 1.

3.2.2 Scenario 2 – Retain PV power production in 2050, but reduce variability

The results of scenario S2 are shown in Figure 12. The top right panel refers to scenario S2-1 calculated with the lowest estimate of 0.891 TW for 2050 by IRENA. The bottom left panel refers to scenario S2-2 calculated with the middle estimate of 1.94 TW for 2050 by Energy Watch Group. The bottom right panel refers to scenario S2-3 calculated with the highest estimate of 8.8 TW for 2050 by SolarPower Europe. Since the latest estimate of 8.8 TW is already higher than the sum of the potential for installed capacity for roof-top mounted PV systems (used as upper bound), we defined the upper bound for this scenario as five times larger. This can be done because free-field PV systems are not considered in the upper bound because free-field PV systems compete with wind turbines. To avoid this trade-off, we only use roof-top mounted PV systems except for scenario S2-3. The installed capacities per country are presented as percentages of the total installed capacity for ease comparison between the three results. The top left panel in Figure 12 shows the upscaled installed PV capacity distribution in 2050. Upscaling is done according to the current percentage of the total IC per country. Since all three plots of the upscaled installed PV capacity distribution for the three used estimates for 2050 would look identical, we only show the plot with the estimate of 1.94 TW. But the total installed capacity and the variability with the three estimates are different and can be found in Table 6, page 38.

The mean change in PV power production from one weather regime to another estimated for 2050 is 5.4% (remains for all upscaled estimates the same because the relative distribution remains constant). Our

method reduced it to 3.3%, 3.6% and 3.5%. This represents a reduction in mean variability of 2.5 GW, 4.7 GW and 22.1 GW, respectively. The maximum change in PV power production from one weather regime to another estimated for 2050 is 16.9% (remains for all upscaled estimates the same because the relative distribution remains constant). This could be reduced to 10.7% (S2-1), 11.9% (S2-2) and 11.6% (S2-3), which refers to a reduction in maximum variability of 7.4 GW, 13.1 GW and 63.0 GW, respectively. An overview of the results can also be found in Table 6, page 38.

In the distributions of S2, South-eastern and North-western countries are still favoured (as in S1). But Spain and Italy also get a share of the capacities. Since the total installed capacities are much higher than in scenario S1, the upper bounds of the countries are more often reached (hatched countries). The method reacts by placing additional capacity in neighbouring countries. This can also be seen by comparing S2-1 (Figure 12, first row) and S2-2 (Figure 12, second row). With higher total installed capacities, the upper bounds are more often reached, and neighbouring countries receive the remaining capacities, and the distribution gets flatter. It goes along with the observation presented in Figure 9, page 28.

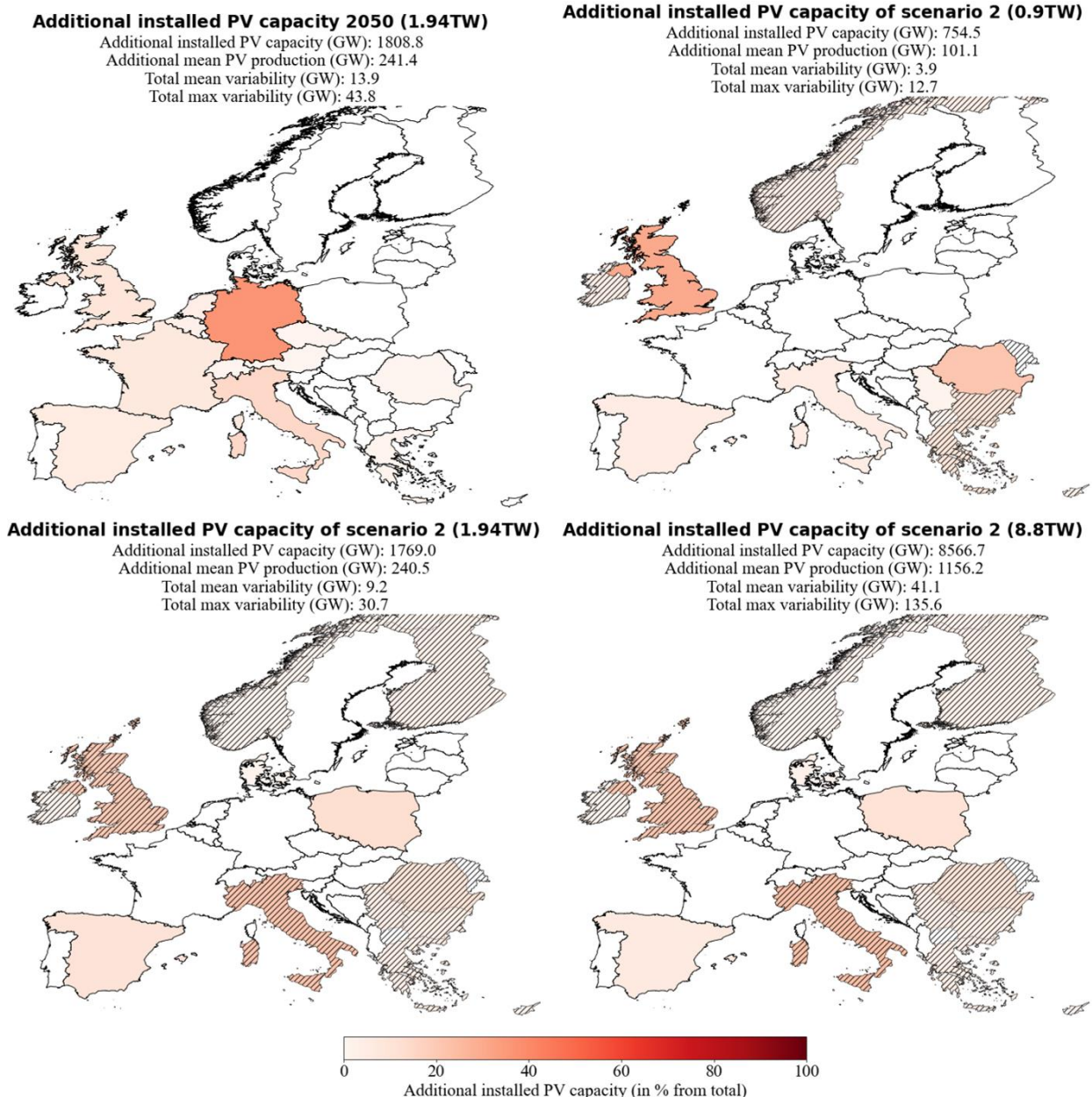


Figure 12: Additional installed PV capacities of 2050 (upscaled from the distribution of 2019) and of scenario 2-1, 2-2 and 2-3. Scenarios 2-1, 2-2 and 2-3 minimize the variability of PV power production with the constraint that the power production must be equal to the PV power production estimated for 2050. The estimated needed total installed PV capacities for 2050 are 0.891 TW, 1.94TW and 8.8 TW. Hatched countries indicate that the upper bound (potential for roof-top mounted PV systems) is reached.

3.2.3 Scenario 3 – Cost and variability minimization

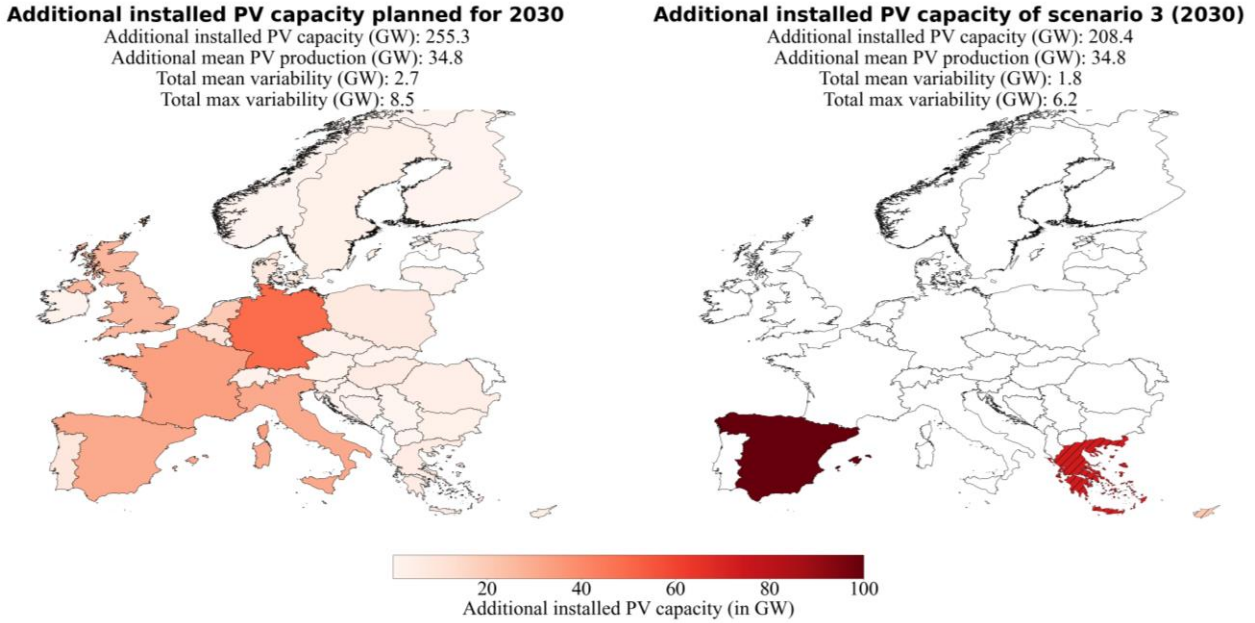


Figure 13: Additional installed PV capacities planned for 2030 (NECPs) and of scenario 3 (S3). S3 minimized the variability of PV power production and the installed PV capacities with the constraint that the power production must be equal to the power production estimated for 2030 (NECPs). Hatched countries indicate that the upper bound (potential for roof-top mounted PV systems) is reached.

With the focus on cost and variability minimisation, we see a shift from the South-Eastern / North-western distribution (S1) to a South-eastern / South-western distribution (Figure 13, second plot). The mean variability could still be reduced from 2.7 GW to 1.8 GW (1.5 GW in S1). This means that the reduction potential for the mean variability gets reduced from 44.4% (S1) to 33.3% (S3). The maximum variability could be reduced from 8.5 GW to 6.2 GW (5.2 GW in S1), which decreases the reduction potential from 38.8% (S1) to 27.1%. The benefit of S3 is that it takes 35.9 GW less installed PV capacity to produce the same amount of electricity compared to S1.

By doing the same analysis with the estimate of 1.94TW for 2050 (Europe Watch Group, S2-2), we get the distribution shown in Figure 14. The method now places all the installed capacities to Southern countries because the capacity factors are generally higher for Southern Europe than Northern Europe (Table 2). The variability can still be reduced with a distribution from the South-West to South-East. The mean variability gets reduced from 13.9 GW to 11.9 GW (9.2 GW in S2-2), and the maximum variability gets reduced from 43.8 GW to 35.0 GW (30.7 GW in S2-2). This decreases the mean variability reduction potential from 33.8% (S2-2) to 14.4% and the maximum variability reduction potential from 29.9% to 20.1%. S3-2 needs 166.8 GW less installed capacity to produce on average 4.4 GW more electricity than S2-2.

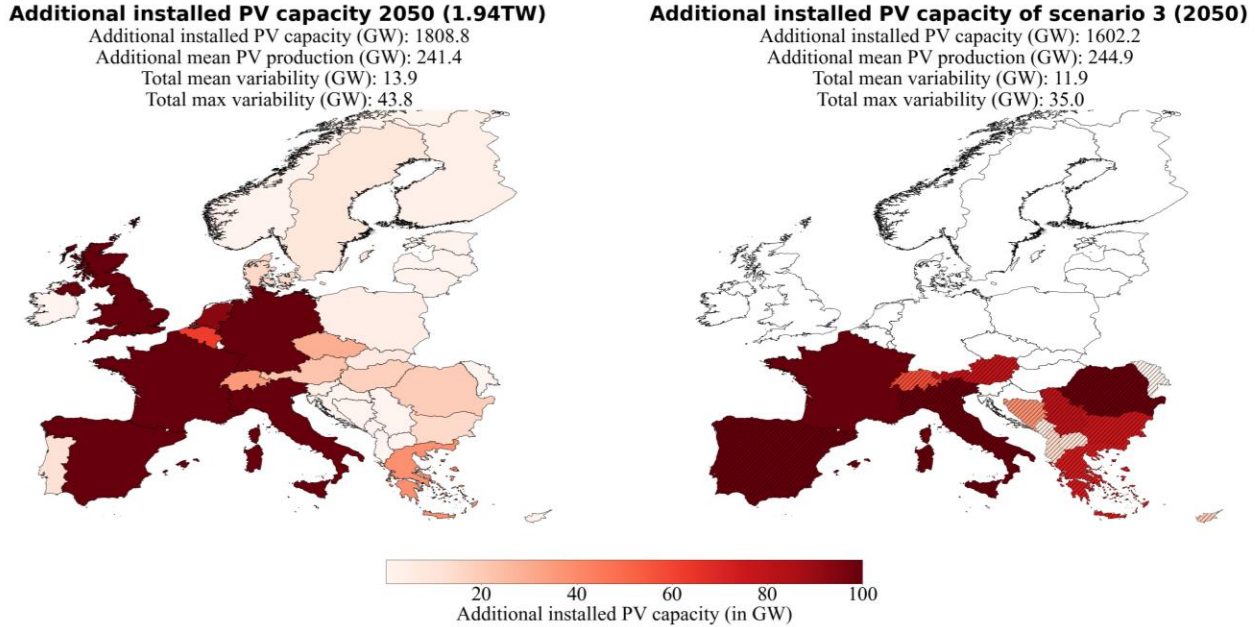


Figure 14: Additional installed PV capacities of 2050 (left panel; upscaled from the distribution of 2019 with the estimate of 1.94 TW installed PV capacity by the Energy Watch Group) and of scenario 3 (S3; right panel). S3 minimized the variability of PV power production and the installed PV capacities with the constraint that the power production must be equal to the power production estimated for 2050. Hatched countries indicate that the upper bound (potential for roof-top mounted PV systems) is reached.

3.2.4 Scenario 4 – Coverage of country-specific electricity consumption

The scenarios examined so far, scenario S1 to S3, ended up with putting more IC to geographically somewhat extreme regions of Europe, like Greece or Scandinavia. In practice, such a distribution of power production would necessitate substantial capacities for power transfer from the production regions to the consumers in other parts of Europe. This motivates investigating yet another scenario where countries want to be self-sufficient to a certain extent. S4-1 enforces this because of the constraint that 10% of the country-specific consumption must be produced with local PV systems in the year 2030. The 10% are chosen because already 13.5% of the total electrical consumption equals the total estimated PV power production for 2030 with the NECPs. This implies that higher coverages than 13.5% can only be achieved with installed PV capacities that produce more power than the estimates for 2030 with the NECPs. And a comparison of the variability with different PV power productions would not be feasible.

The results are shown in Figure 15. All countries get their needed installed capacities to cover 10% of their consumption, and the rest is again distributed to South-eastern and North-western Europe. The flatter distribution is at the expense of the variability reduction potential. It reduces from 44.4% (S1) to 29.6% for the mean variability and reduces from 38.8% to 29.4% for the maximum variability. This means that we reduce the total mean variability from 2.7 GW to 1.9 GW (1.5 GW in S1) and the total maximum variability from 8.5 GW to 6.0 GW (5.2 GW in S1).

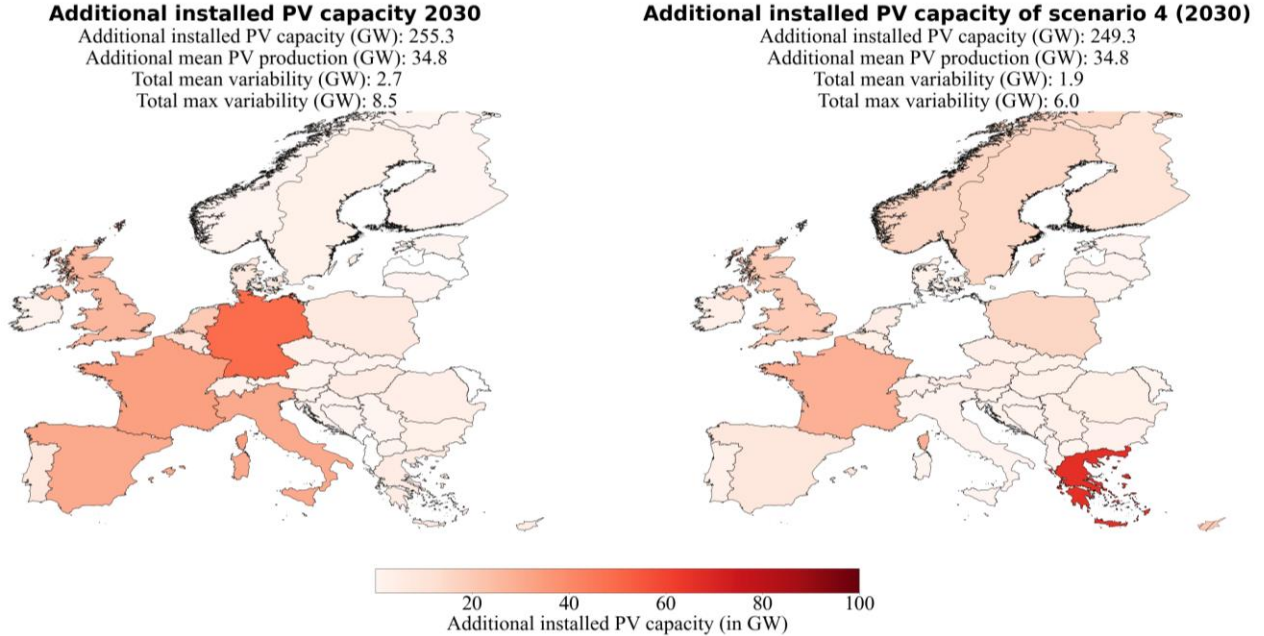


Figure 15: Additional installed PV capacities planned for 2030 (NECPs) and of scenario 4-1 (S4-1). S4-1 minimized the variability of PV power production with the constraint that the PV power production must be equal to the PV power production estimated for 2030 (NECPs) and 10% of the inland electricity consumption must be covered with PV power production by the countries themselves.

The same analysis but with the estimate of 1.94 TW installed capacity for 2050 by the Energy Watch Group and the constraint that 30% of the consumption per country must be covered with PV power production yields the results presented in Figure 16. The flatter distribution is again at the expense of the mean variability reduction potential. It decreases from 33.8% (S2-2) to 28.1%, a reduction from 13.9 GW to 10.0 GW (9.2 GW in S2-2). Interestingly the maximum variability reduction potential increases within this scenario from 29.9% (S2-2) to 30.4%, which is a reduction from 43.8 GW to 30.5 GW (30.7 GW in S2-2).

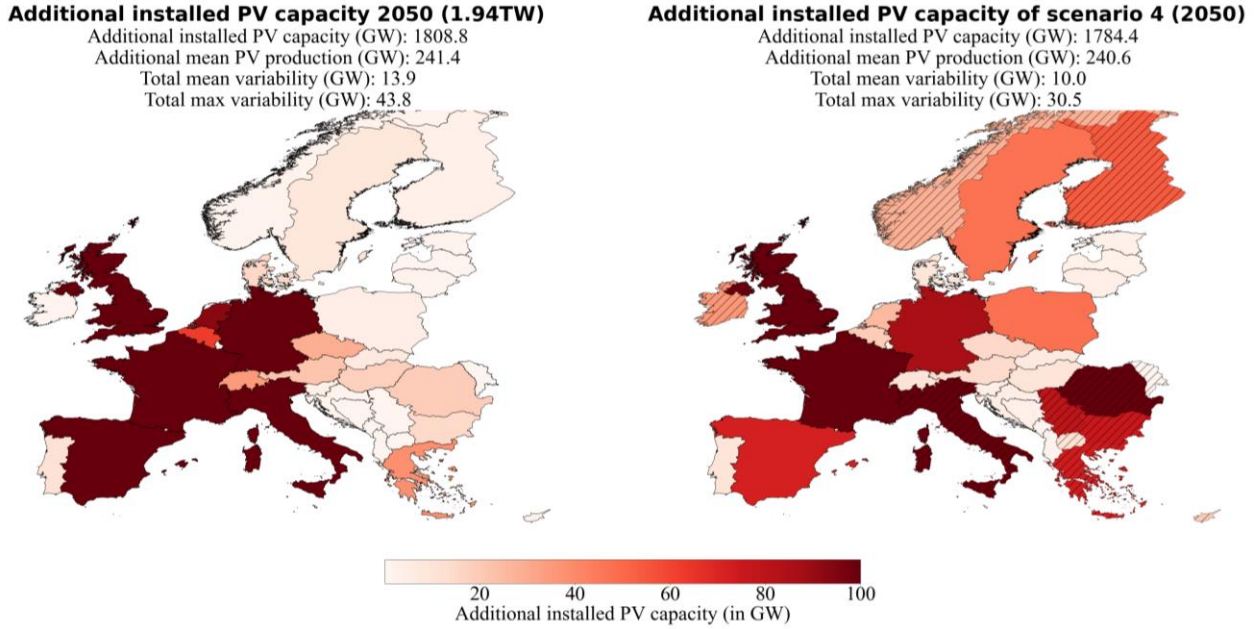


Figure 16: Additional installed PV capacities of 2050 (upscaled from the distribution of 2019 with the estimate of 1.94 TW installed PV capacity by the Energy Watch Group) and of scenario 4-2 (S4-2). S4-2 minimized the variability of PV power production with the constraint that the PV power production must be equal to the PV power production estimated for 2050 and 30% of the inland electricity consumptions must be covered with PV power production by the countries themselves. Hatched countries indicate that the upper bound (potential for roof-top mounted PV systems) is reached.

An overview of all the four scenarios' important results can be found in Table 5 and Table 6. They have separated into all results for 2030 (Table 5) and all results for 2050 (Table 6) to facilitate comparisons between the different scenarios for the same year. A detailed analysis of the over- and underproductions for every weather regime and season compared to their seasonal mean and the consolidated view of the variabilities for every scenario can be found in the Appendix (Figure 17 - Figure 29).

Table 5: Overview of all the important variables of the three scenarios of the year 2030 and their reference data. Scenario S1 is only constrained by equal PV power production. Scenario S3-1 is constrained by equal PV power production and cost minimization. Scenario S4-1 is constrained by equal PV power production and that 10% of the country-specific consumption must be produced with PV systems.

| | 2019 | NECPs 2030 | S1 2030 | S3-1 2030 | S4-1 2030 |
|---|-------|---------------|------------|--------------|--------------|
| Installed PV capacity [GW] | 131.2 | 386.5 | 375.5 | 339.6 | 380.4 |
| Mean PV production [GW] | 17.5 | 52.3 | 52.2 | 52.3 | 52.3 |
| Mean variability [GW] | 0.9 | 2.7 | 1.5 | 1.8 | 1.9 |
| Maximum variability [GW] | 3.0 | 8.5 | 5.2 | 6.2 | 6.0 |
| Mean variability / Mean PV production [%] | 5.1% | 5.2% | 2.9% | 3.4% | 3.6% |
| Maximum variability / Mean PV production [%] | 17.1% | 16.3% | 10.0% | 11.9% | 11.5% |
| Mean variability reduction [GW] | - | - | 1.2 | 0.9 | 0.8 |
| Maximum variability reduction [GW] | - | - | 3.3 | 2.3 | 2.5 |
| Mean variability reduction [%] | - | - | 44.4% | 33.3% | 29.6% |
| Maximum variability reduction [%] | - | - | 38.8% | 27.1% | 29.4% |

Table 6: Overview of all the important variables of the three scenarios for 2050 and their reference data. Scenario 2-1 to 2-3 are constrained by equal PV power production. Scenario S3-2 is constrained by equal PV power production and cost minimization. Scenario 4-2 is constrained by equal PV power production and that 30% of the country-specific consumption must be produced with PV systems.

| | 2050 0.891 TW | 2050 1.94 TW | 2050 8.8 TW | S2-1 (2050) 0.891 TW | S2-2 (2050) 1.94 TW | S2-3 (2050) 8.8 TW | S3-2 (2050) 1.94 TW | S4-2 (2050) 1.94TW |
|---|------------------|-----------------|----------------|-------------------------|------------------------|-----------------------|------------------------|-----------------------|
| Installed PV capacity [GW] | 891.0 | 1940.0 | 8800.0 | 885.6 | 1900.2 | 8697.8 | 1733.4 | 1915.6 |
| Mean PV production [GW] | 118.9 | 258.9 | 1174.4 | 118.6 | 258.0 | 1173.7 | 262.4 | 258.1 |
| Mean variability [GW] | 6.4 | 13.9 | 63.2 | 3.9 | 9.2 | 41.1 | 11.9 | 10.0 |
| Maximum variability [GW] | 20.1 | 43.8 | 198.6 | 12.7 | 30.7 | 135.6 | 35.0 | 30.5 |
| Mean variability / Mean PV production [%] | 5.4% | 5.4% | 5.4% | 3.3% | 3.6% | 3.5% | 4.5% | 3.9% |
| Maximum variability / Mean PV production [%] | 16.9% | 16.9% | 16.9% | 10.7% | 11.9% | 11.6% | 13.3% | 11.8% |
| Mean variability reduction [GW] | - | - | - | 2.5 | 4.7 | 22.1 | 2.0 | 3.9 |
| Maximum variability reduction [GW] | - | - | - | 7.4 | 13.1 | 63.0 | 8.8 | 13.3 |
| Mean variability reduction [%] | - | - | - | 39.1% | 33.8% | 35.0% | 14.4% | 28.1% |
| Maximum variability reduction [%] | - | - | - | 36.8% | 29.9% | 31.7% | 20.1% | 30.4% |

4. Discussion

Our results suggest that with the derived seven weather regimes for Europe, it is possible to assess PV power production variability year-round. With that as a basis, we estimated how PV power production variability could change as its deployment proceeds in the years 2030 and 2050. We introduce a novel method to numerically find a spatial distribution of installed PV capacities, which reduces the PV power production variability related to changing weather regimes. The four scenarios' derived results emphasize how readily the method can be extended to implement additional constraints. In the following section, we put the obtained results into the context of existing literature, discuss the findings of this study and its possible implications and hint at limitations. We start with the weather regime classification, as they form the basis for any further analysis, then proceed to WR-associated PV production and its variability under present-day conditions. Finally, we return to this study's initial motivation to answer the following question: In a future where renewables will dominate energy production, to what degree can WR-associated variability of PV power production be counteracted by an optimized spatial distribution of future PV systems?

4.1 Comparison to past work

4.1.1 Weather regimes classification

As the weather regimes are the basis for our analysis, we first need to see how our results compare with the literature if we want to compare PV power variability with the literature. Although the weather regime classification is year-round, our defined seven weather regimes include the four weather regimes which are found by many studies that focused only on wintertime weather regime classification (Cassou, 2008; Michelangeli et al., 1995; van der Wiel et al., 2019; Vautard, 1990): The positive phase of the NAO (WR0), the negative phase of the NAO (WR2), the Atlantic ridge (WR3) and the Scandinavian blocking (WR6). Their frequencies (Figure 6 and Appendix Table 8) suggest that we are in line with these studies because they occur most often in winter, except the Scandinavian blocking. The most likely explanation for this is that the European blocking belongs to the top four weather regime during wintertime in our analysis instead of the Scandinavian blocking. Since these two weather regimes are similar, one might be at the other's expense because we split them into two separate weather regimes.

A comparison with the seven weather regimes defined year-round by Grams et al. (2017) shows that they mostly agree with our weather regime classification. Their results also include the four already discussed weather regimes with a slightly different naming convention. WR0 (NAO+) matches with Grams et al. (2017) zonal regime, and WR2 (NAO-) matches with their Greenland blocking. The Scandinavian blocking (WR6) and the Atlantic ridge (WR3) have the same naming convention. Contrary to our frequencies during wintertime, Grams et al. (2017) frequencies do not determine them as the most frequent ones in winter. Overall, the frequency of occurrence per weather regime is similar but usually somewhat

lower in Grams et al. (2017) study, which, by contrast, have a larger share of no regime. In addition to those four weather regimes, Grams et al. (2017) used the three weather regimes Atlantic trough, European blocking, and Scandinavian trough. European blocking is in line with our findings. In contrast, the Scandinavian trough in his study is primarily comparable with the European trough in our study. But as the names state, the cyclone in Grams et al. (2017) is located over Scandinavia and, in our study, over North-western Europe. Additionally, the meridional dipole is more pronounced in our results. The Atlantic trough is in good agreement with Grams et al. (2017) results. But the positive geopotential height anomaly in Southern Europe in our study is more pronounced. The differences are most likely explained because some details within Grams et al. (2017) chosen method to classify the weather regimes differ from ours. The difference in the definition of the reference climatology (30- vs 90-day running mean) and the differences in the assignment of days to no regime should be emphasized here. Overall, the weather regimes classification follows findings reported by others (Cassou, 2008; Grams et al., 2017; Michelangeli et al., 1995; van der Wiel et al., 2019; Vautard, 1990).

4.1.2 Capacity factor anomalies and surface weather variables

Having shown that the weather regime classification agrees with the literature, we compare weather regime dependent quantities across studies. The surface weather variable anomalies (solar radiation and 2m temperature) and as a direct consequence, the CFs anomalies are in good agreement with other studies. The four well-studied weather regimes in wintertime are especially in line with previous results (Bloomfield et al., 2020; Grams et al., 2017; Jones et al., 2020; Pozo-Vazquez et al., 2011; van der Wiel et al., 2019). We present a more detailed discussion about the seven weather regimes in the following seven paragraphs.

The **positive phase of the NAO (WR0)** suggests a negative correlation to the surface solar radiation anomalies in Northern Europe and a positive correlation in Southern Europe (Figure 4). Consequently, CF anomalies behave similarly: During the positive phase of the NAO, Southern Europe experiences a relative surplus in PV power production, whereas PV power production is below average in Northern Europe. The correlation between NAO+ and surface solar radiation is in agreement with the study by Pozo-Vazquez et al. (2011), although it is disputed by Colantuono et al. (2014). The observed North-South gradient of the PV CF anomalies can also be observed in Grams et al. (2017). And the changes throughout the seasons are consistent with them as well. Van Der Wiel et al. (2019) study, which only focuses on wintertime, stated that the surface solar radiation is close to normal during the NAO+. But a slightly North-South gradient can also be observed in their results. Our results partly agree with those, as the discrepancy between North and South decreases in winter compared to the rest of the year.

The observed negative correlation between the **negative phase of the NAO (WR2)**, the surface solar radiation, and the CFs anomalies in Northern Europe (negative correlation for Southern Europe) tends to be more robust. This also applies to the observed overall negative temperature anomaly in Europe (Grams

et al., 2017; Hurrell et al., 2003; Jerez et al., 2013; Pozo-Vazquez et al., 2011; van der Wiel et al., 2019). Van der Wiel et al. (2019) identified that the combination of low temperature and lower than average wind speed during the NAO- is at the risk that the demand for electricity increases the supply of electricity in Europe. Since the CF are enhanced during NAO- in Northern Europe, it might be possible to reduce that risk with additional installed PV capacities in this region.

The enhanced surface solar radiation and capacity factor anomalies in South-western Europe during the **Atlantic ridge (WR3)** matches well with Grams et al. (2017) and van der Wiel et al. (2019). Nevertheless, the temperature anomalies in winter found by van der Wiel et al. (2019) are less pronounced than our temperature anomalies defined year-round. But the changes throughout the season of the CF anomalies are relatively big, which gives reason to assume that the surface weather variables also do. Our identified changes throughout the seasons are primarily in line with Grams et al. (2017).

The anticyclone over Scandinavian during the **Scandinavian blocking (WR6)** brings higher than normal surface solar radiation to Northern Europe. The enhanced surface solar radiation caused by descending air and therefore clear sky condition is in line with Amajama (2016) study. The resulting higher than average 2m temperature and CFs anomalies, which is relatively constant for all seasons, are also observed by Grams et al. (2017) and van der Wiel et al. (2019).

These observations also hold for the **European blocking (WR5)**. Generally, we see enhanced surface solar radiation anomalies and therefore enhanced CF anomalies in Central Europe where the Anticyclone is located (in line with Amajama, (2016)). The seasonal change is more pronounced, which partly agrees with Grams et al. (2017). The shift from slightly positive CFs anomalies in Southern Europe in winter to slightly negative values in summer fits the observation by Grams et al. (2017). In contrast, they do not agree with Northern countries. As presented earlier, we found that the CF anomalies are slightly negative in winter, whereas, on the other hand, Grams et al. (2017) found strongly positive values. The reason for the difference is not yet clear. One could argue that the seasonal cycle has a strong influence during this weather regime in our study. Positive CF anomalies in winter are most pronounced in Southern Europe. But a northward shift towards summer can be observed and again a southward change in autumn, which is likely to be explained by the seasonal cycle of surface solar radiation. This obvious and strong influence of the seasonal cycle cannot be observed in the other weather regime and their CF anomalies.

The surface solar radiation and CF anomalies of the **European through (WR1)** do agree to a large extent with the Scandinavian through defined by Grams et al. (2017). Also, the changes throughout the season match well. Main differences arise from Southern countries, which tend to be more negative within our study in wintertime. This could be explained by the cyclone's position, which in our results are located more to the South. A comparison with the study by Jones et al. (2020), which investigated the impact of 29 Grosswetterlagen on the European Energy Sector, show that the PV power production anomalies of the

Grosswetterlage TRW (through Western Europe) and TM (through Central Europe), which are mostly comparable with the European through from our analyses, are more in line with our results.

The **Atlantic trough (WR4)** is the weather regime that agrees the least with the weather regimes defined by Grams et al. (2017). This is mainly because of the positive geopotential height anomaly in Southern Europe, which is more pronounced in our results. Therefore, it could be expected that the CFs anomalies and weather variables also do not fit well. Indeed the surface solar radiation and the CF anomalies in South-eastern Europe are higher than average within our study, contrary to those reported by Grams et al. (2017). This is more in line with the study by Jones et al. (2020), which also suggest positive solar power production anomalies in South-eastern Europe during the Grosswetterlagen SWZ (cyclonic South-westerly) and SWA (anticyclonic South-westerly), which are relatable to the Atlantic trough. The negative surface solar radiation anomalies observed by Grams et al. (2017) for Northern countries fit again with our observed surface solar radiation anomalies. And the negative CF anomalies in Northern Europe in winter are in good agreement. But our results suggest that the already more positive CF anomalies in South-eastern Europe extend northwards during spring and autumn. This partly agrees with Grams et al. (2017), where the CF anomalies increase towards summer.

4.1.3 Current and projected PV power production variability

Since the power production of PV is still relatively small compared to wind power production in Europe, few studies focus on its variability. Therefore, we mainly compare our results with the study by Grams et al. (2017), which analysed its current variability but did not further investigate its reduction potential for the same reason. An overview of the comparison between our and Grams et al. (2017) results can be found in Table 7, presented so that the total installed PV capacity difference is considered (131.2 GW in 2019 vs 87.91 GW in 2015).

Table 7: Comparison of PV power production and variability with the study by Grams et al. (2017). The PV power production (2019) estimated within this study is divided by the installed capacity of 2019 (131.2 GW). The PV power production estimated by Grams et al. (2017) is divided by the installed capacity of 2015 (87.91 GW). This is done to make a comparison feasible. The same is done for the obtained maximum variability and PV power production of this study and the study by Grams et al. (2017).

| | Winter | Spring | Summer | Autumn |
|--|--------|--------|--------|--------|
| PV power production / installed PV capacity 2019 | 6.6% | 16.5% | 19.6% | 10.7% |
| PV power production / installed PV capacity obtained by Grams et al. (2017) | 6.8% | 16.7% | 19.7% | 10.9% |
| Maximum variability / PV power production 2019 | 19.3% | 13.6% | 6.8% | 21.1% |
| Maximum variability / PV power production obtained by Grams et al. (2017) | 31.8% | 17.7% | 5.1% | 23.8% |

The PV power production divided by the PV installed capacity is nearly identical. This could be expected since the data source for the CF are the same, and the percentual distribution of installed capacities from 2015 to 2019 in Europe did not change dramatically. Although the change in the percentual distribution has not changed much, it might explain the results' slight differences.

The maximum variability divided by the PV power production does not fit as well as the PV power production divided by the installed PV capacity. The pattern from spring, to summer, to autumn, are alike and generally of similar sizes. In spring, it amounts in our study to 13.6%, whereas for Grams et al. (2017) it is 17.7% (Table 7). In summer (6.8% vs. 5.1%) and autumn (21.1% vs 23.8%) they are even more similar. But the maximum variability divided by the PV power production for winter shows a greater difference (19.3% vs 31.8%). The reason is not yet clear. But since PV power production and therefore also the absolute variability are lowest in winter anyway, it might play a less important role for general variability optimization considerations.

4.2 Dangers of increased variability

While PV power production is still of minor importance compared to total power production, this will increasingly change. Once PV power production contributes substantially to total power production, the relative variabilities in Table 5 and Table 6 become significant. Grams et al. (2017) stated that a tenfold PV installed capacity increase is required to be comparable with the variability caused by wind turbines. According to the plans by NECPs, installed PV capacity already triples in 2030. Our results suggest that this could lead to a variability of 8.5 GW (about 8 to 9 present-day nuclear power plants), which corresponds to 16% of the foreseen wind power production variability of 51.7 GW in 2030 (Grams et al., 2017). The estimates for a 100% renewable energy – power sector by the Energy Watch Group, which is the source for our scenario S2-2, suggest that the PV installed capacity must increase 19 times from 2015 until 2050. Simultaneously, a four-fold increase is estimated for wind installed capacity. This shows that towards 2050 PV power production becomes more important. As shown in S2 (Table 6), this could lead to a PV power production variability from 20.1 GW up to 198.6 GW in the year 2050, which is of comparable size to the 89.6 GW wind power production variability that we get if we simply upscale the variability estimates by Grams et al. (2017).

As mentioned above, with the current planning strategies for 2030, energy system operators will need to consider the fluctuation of 8.5 GW electric power caused by PV. In 2050 this could massively increase from 20.1 GW to 198.6 GW, depending on the scenario. The electricity demand must always equal electricity production to ensure a stable power grid. This study neglected the electricity demand since the focus is on PV power production variability. Others (Bloomfield et al., 2020; van der Wiel et al., 2019) analysed the energy system's stress caused by wind and PV production and their dependency on weather. They determined that blocking situations on average have lower than average power production with wind

and PV, and higher than average energy demand. Our results suggest that PV power production is contrariwise higher on average during blocking situations. E.g., during the European blocking (WR5), PV power production is usually highest. In contrast, it is lowest for wind power production (Grams et al., 2017). The stress for the energy system during blocking situations can be explained by the fact that wind power production is still dominating over PV power production and therefore determines the production pattern. That highlights the potential to reduce the energy system's stress if PV power production becomes more competitive to wind power production. The anticorrelation between wind and PV power production can help to balance the electricity grid.

A closer look at the weather regimes with the highest overproduction shows that it always occurs during WR5 (European blocking) except for winter, during WR6 (Scandinavian blocking). This is in line with Grams et al. (2017), which also report the highest overproduction, mainly during blocking situations. The lowest underproduction always occurs during WR1 (European through). An overview of the over- and underproduction per weather regime and season can be found in Figure 10 and Appendix Table 9. It is worth mentioning that if a weather regime exhibits over- or underproduction, it does so throughout the season. This gives rise to group the weather regimes accordingly. Weather regimes with a positive geopotential height anomaly (anticyclone, blocking) over the Atlantic or Continental Europe (WR3, WR4, WR5 and WR6) usually exhibits overproduction (expect WR4 winter and WR3 summer). The positive and negative phase of the NAO (WR0 and WR2) or weather regimes with negative geopotential height anomalies over Europe (cyclone) usually exhibit underproduction (expect WR0 summer). These general over- or underproduction patterns show that there are weather regimes where a reduction of PV power production variability is not possible. The method aims to align the PV power production per weather regime and season to the mean PV power production per season. But for weather regimes like, e.g. WR1, which has negative CF throughout the whole season almost everywhere, this is not feasible. In other words, a gradient of the CF anomalies throughout Europe is needed that the method can achieve its aim of reducing the PV power production variability. If there is no gradient of the CF anomalies throughout Europe, the variability must be balanced from other sources. For instance, wind power production exhibits an anticorrelation to PV power production and could be used for this purpose (Grams et al., 2017). It also leads to the general question of balancing the variable power production of renewable technologies. Because even with an optimized spatial distribution of wind turbines and PV systems, a certain amount of variability will always remain, which needs to be balanced. That highlights the importance of further expanding storage possibilities (battery, hydrogen, pumped-storage hydroelectricity, synthetic fuel, to name a few), which are needed to run a stable power grid in a fossil-free electricity-producing future.

4.3 Opportunities to decrease variability

In line with other studies, the present work shows that PV power production in Europe undergoes substantial variability on time scales of several days due to weather regimes. Two basic situations can further be distinguished: weather regimes associated with both over- and underproduction of PV power production in different parts of Europe and weather regimes associated with an overall over- or underproduction throughout Europe. In the former case, our study shows that suitable spatial deployment of PV panels can substantially reduce the weather regime associated variability of PV power production, as further discussed below in Sections 4.3.1 to 4.3.4. In the latter case, the spatial distribution of PV systems is shown to help little, and weather regime associated variability must be counteracted by other means.

The four scenarios suggest that the objective of reducing PV power production variability can be addressed by adding future installed PV capacities to South-eastern and North-western Europe. Visual analysis of the classified seven weather regimes goes along with these results. High and low geopotential height anomaly fields are either affecting half of Europe (e.g. WR0), often with a South-east/North-west gradient, or entire Europe with decreasing intensity on the edges (e.g. WR5). It also goes along with the anomalies of surface solar radiation and 2m temperature. Especially the distribution of surface solar radiation often shows a discrepancy between South-eastern and North-western Europe. And it still holds for the CF anomalies, but the distribution shifts a bit, and the discrepancy between North and South is more pronounced than East to West. This indicates that the CF pattern associated with the different weather regimes are fair although not entirely robust to season.

4.3.1 Scenario 1 – Retain PV power production in 2030, but reduce variability

The estimates of S1 show that the potential of reducing mean and maximum variability is 44.4% and 38.8%, respectively. These are the highest percentual reduction for the mean and maximum variability achieved within our four scenarios (Table 5 and Table 6). It highlights to which extent it is possible to reduce the PV power production variability since the only constraint in this scenario is minimum PV power production (which has to equal to the PV power production estimated for 2030). A closer look at the variability per season and weather regime (Figure 10) shows that the seven cases (out of 32) where the deviation of PV power production from the seasonal mean could not be reduced are often related to WR4. For spring and summer, it was exclusively WR4 which could not be reduced. The changes throughout the season of WR4 (Figure 5) might explain why it is difficult to reduce the deviation of PV power production from the seasonal mean for this weather regime. In winter, the CF anomalies have the typical South-eastern / North-western pattern, which explains why the deviation from the seasonal mean nearly vanishes in winter with the IC distribution found in S1. But the CF anomalies in the rest of the seasons are generally more positive (especially in spring) and no longer a distinctive South-eastern / North-western pattern.

Three of the seven cases where PV power production variability could not be reduced occur in winter. Interestingly WR4 is not one of them, and the deviation from the seasonal mean of it could be reduced to nearly zero. The reason why winter is the season in which most of these seven cases occurs might be because PV power production is generally lowest in winter. Since the linear least-square problem reduces the sum of the absolute deviation from the seasonal mean for each weather regime and season, winter with its lower PV power production is just less important than others. Unfortunately, winter is the season where electricity demand is highest, and therefore PV power production variability plays an important role.

4.3.2 Scenario 2 – Retain PV power production in 2050, but reduce variability

From scenario two, it is clear how important PV power production variability could become towards 2050. Depending on the projected installed PV capacity for 2050, the maximum variability reaches a value between 20.1 GW and 198.6 GW. This is roughly up to 20 times larger than the estimates for 2030. Since the reduction potential achieved with our optimized distribution is just slightly lower in S2 than S1, the saved up needed balancing electricity is also roughly 20 times larger. One would need the electricity produced by up to 60 nuclear power plants less to balance the power grid. An important implication of these findings is that before further massive deployment of PV systems, one must consider if the cost for balancing the difference of these variabilities is higher or lower than the cost that would arise by investing in expanding the current power grid to ensure its transmission.

The distribution of S2 (Figure 12) goes along with the distribution of S1. South-eastern and North-western countries are still favoured. But since the total installed PV capacities have increased, the upper bound of countries are more often hit (e.g. Romania), and other countries like Italy and Spain get higher installed capacities. This indicates that at some point, the variability reduction potential is no longer best addressed by adding the installed capacities to South-eastern Europe. The results suggest that this point is reached as soon as Greece and Bulgaria are (almost) at their upper bound. Afterwards, the method starts to place the installed capacities in Spain (already in S1) and Italy. A similar observation is presented in scenario S1, Figure 9, page 28.

The achieved reduction potentials of S2 are slightly lower than the reduction potential of S1. As mentioned, with the higher defined installed PV capacity of S2, the countries' upper bound are more often hit. Therefore, the method places the installed capacities elsewhere, which comes at the expense of the variability. It can nicely be seen by comparing S2-1 and S2-2 (Figure 12 and Table 6), where the installed capacities are different, but the upper bounds remain. The mean variability reduction decreases about 5.3%, and the maximum variability decreases about 6.9% (from S2-1 to S2-2).

The distribution and reduction potential of S2-3 and S2-2 are similar because we increased the upper bounds by three times in scenario S2-3. As mentioned, this has been done because the sum of the total installed capacity of the upper bound is already lower than the highest installed capacity estimated for 2050

of 8.8 TW. One interpretation of this finding is that if the upper bounds and the installed capacity are increased similarly (the installed capacity of S2-3 is also roughly increased five times compared to S2-2), the distribution and reduction potential remains unchanged. This might lead to a general optimal distribution pattern that could linearly increase with increasing installed capacities as long as the upper bounds are not hit. Remarkable is also that the potential of roof-top mounted PV systems (Tröndle et al., 2019) is smaller than the highest estimates of needed installed PV capacity for 2050. This highlighting the importance of free field mounted PV systems.

4.3.3 Scenario 3 – Cost and variability minimization

The findings of scenario three highlight that reducing PV power production variability does not strongly conflict with lowering costs. Instead, it is possible to achieve the same PV power production with 18% less additional installed PV capacity while still decreasing the PV power production variability (S3-1, Figure 13 and Table 5). And the mean and maximum reduction potential of 33.3% and 27.1% is even within reach of S1 and S2. But the distribution to only three countries (Cyprus, Greece, and Spain) also show its limit.

S3-2 suggests that it is harder to reduce the PV power production variability with higher total installed PV capacity and cost reduction considerations. A reduction in the variability could still be achieved but decreases drastically to roughly a quarter of the mean reduction potential and half of the maximum reduction potential of S2-1. The benefit in reducing the cost has also decreased. S3-1 could produce the same amount of electricity with 18% less additional installed PV capacity. In S3-2, it decreases to 11%. The reason is probably again because the upper bounds are more often hit. This can also be seen in Figure 14 (right plot), where nearly all Southern countries are at their upper bound.

4.3.4 Scenario 4 – Coverage of country-specific electricity consumption

The enforcement of a flatter distribution in S4, by the constraint that a certain amount of electricity consumption must be produced with PV by every country itself, indicates that a reduction of the variability is still feasible although its potential is lowered. The reduction potential estimated for 2030 and 2050 is nearly identical. The most likely explanation is that in S4-1, 10% of inland electricity consumptions must be covered with PV systems and S4-2 30%. An interesting side note within this scenario is that 13.5% of the current total electricity consumption of Europe is equal to the PV power production estimated with installed PV capacity planned for 2030. The results of S4 may be of interest when planning larger solar systems and their location. Even in an already present flat installed PV capacity distribution, a new large solar system in a key country like Greece could reduce the PV power production variability. Additionally, the flatter distribution has the impact that the need to exchange electricity over power lines is reduced.

4.4 Limitations

This study has some possible limitations, which are consolidated in this section. The first is neglecting the transmission of electricity. We assume that it is possible to produce electricity at one location in Europe and use it somewhere else without considering the limitations of the current power grid. Our results suggest placing additional PV systems in North-western and South-eastern Europe to reduce the variability. This implies that the transport of electricity from these locations to the rest of Europe must be possible. Otherwise, it cannot be used for balancing purposes. The main reason to neglect the transmission is that this study's focus lies in the potential of reducing PV power production variability. There is the basic information of PV power production variability for further planning strategies towards a fossil-free electricity generation future. It can be used as a factor to assess whether the expansion of the European power grid is worthwhile.

Another limitation is that we only focus on weather regime related PV power production variability. But weather regime associated variable power production is an issue that also affects other renewable energy technologies. Additionally, the impact of PV power production variability goes hand in hand with electricity demand and storage possibilities. Since PV power production is just one part of variability considerations, our study misses the opportunity of a combined analysis with other components of the energy system.

The third limitation is related to spatial scaling. The use of country-specific PV capacity factors might underrepresent spatial differences in large countries. It could also mask the difference of PV capacity factors within one country during a specific weather regime. For instance, in WR3, we see a gradient of surface solar radiation and 2m temperature from western to eastern Spain. This difference is averaged out by using one CF for Spain.

Finally, our results indicate that the CF patterns associated with the weather regimes are fairly but entirely robust to season. It might be possible to further increase the robustness to the season by analysing monthly CF instead of seasonal CF.

5. Conclusion & Outlook

PV power production is subject to significant fluctuations because of its dependency on weather conditions. Currently, the fluctuations are still of minor importance to the power grid because PV power production in Europe is still small compared to the power produced by other technologies. Therefore, little attention has been paid to its variable production pattern until now. But with the growth of installed PV capacity, the weather-dependent variability becomes essential. To quantify its current and future possible impact on the energy system, we have assessed the PV power production variability based on weather regime classification and country-specific PV capacity factors. Using the National Energy and Climate Plans of European countries, we have projected the variability in 2030. Also, estimates for 2050 have been calculated using different fossil-free electricity-producing scenarios. This fulfils the first aim of this study to assess current and project future PV power production variabilities. Moreover, we have achieved the study's second aim by introducing a numerical method, showing the potential of reducing PV power production variability with an optimized distribution of PV systems in Europe. To our knowledge, this is the first study to examine the reduction of PV power production variability with a distribution of PV systems based on weather regime classification.

We have estimated that already in 2030, the change in PV power production from one weather regime to another could amount to up to 8.5 GW. Consequently, other power plants or storage facilities must generate this electricity to balance the power grid. To put this into context, roughly eight nuclear power plants are needed to produce this amount of electricity. We have shown that under the condition of an unlimited power grid (transmission), a South-eastern/North-western distribution of PV systems in Europe can reduce this variability by roughly 40% to 5.2 GW. Furthermore, the investigations indicate that PV production variability and costs can be reduced simultaneously. It is feasible to reduce the variability projected to 2030 by roughly 30% with 10% less installed PV capacity. Different studies propose that the installed PV capacity must increase massively towards 2050 if we want to achieve a 100% renewable electricity-producing Europe (IRENA, 2020a; Ram et al., 2017; SolarPower Europe and LUT University, 2020). Based on these studies, we have estimated the maximum variability in 2050 from 20.1 GW up to 198.6 GW. We could reduce it with an optimized distribution by roughly one third. In those scenarios foreseeing large PV capacity additions, the potential of roof-top mounted PV system per country is repeatedly reached, and our method places additional installed PV capacities to countries where the variability reduction potential is smaller. Not being able to exploit the optimal locations lowers the potential to reduce the variability from 40% (2030) to 30% (2050). Nevertheless, in absolute numbers, this 30% yields a substantial reduction of 7.4 up to 63 GW. This implies that with an optimised distribution of PV systems, we wouldn't need the electricity that roughly corresponds to the production of seven up to 60 nuclear power plants to balance the power grid. Additionally, we could show that it is also feasible to reduce the variability

and the costs simultaneously with the estimates for 2050. With 10% less installed PV capacity, we could reduce the variability by roughly 20%.

We have shown that as the installed PV capacity increases in the future, the associated variability in power production becomes substantial in absolute amount. This suggests that before further massive deployment of PV systems, it is worth considering the potential that lies in an optimized distribution of PV systems within Europe. The study presents first concrete suggestions in that direction. If we do not take this opportunity, the variable power input will be unnecessarily more extensive, and more research and innovation are needed to balance the power grid sustainably.

The issue of variable power production with renewable energy technologies is a broad field in space, time and technology, and this study shows one crucial example of it. A specific aspect for further work is to use the anticorrelation between wind and PV power production. Since our method is easily extendable, it is worth adding the wind capacity factors and find a combined PV systems and wind fleets distribution that reduces power production variability. Another improvement of the presented method could be to use capacity factors on a smaller scale than country-specific ones. One can imagine that in a large country like Germany, the capacity factors in the South differ significantly from the capacity factors in the North. An analysis on a smaller scale would take that into account and increase the number of locations where PV systems can be distributed.

6. References

- Amajama, J. (2016). Effect of Air Pressure on the Output of Photovoltaic Panel and Solar Illuminance (or Intensity). *International Journal of Scientific Engineering and Applied Science*, 2(8), 139–144.
- Baur, F., Hess, P., & Nagel, H. (1944). *Kalender der Großwetterlagen Europas 1881–1939*.
- Bloomfield, H. C., Brayshaw, D. J., & Charlton-Perez, A. J. (2020). Characterizing the winter meteorological drivers of the European electricity system using targeted circulation types. *Meteorological Applications*, 27(1), 1–18. <https://doi.org/10.1002/met.1858>
- Branch, M. A., Coleman, T. F., & Li, Y. (1999). Subspace, interior, and conjugate gradient method for large-scale bound-constrained minimization problems. *SIAM Journal of Scientific Computing*, 21(1), 1–23. <https://doi.org/10.1137/S1064827595289108>
- Brayshaw, D. J., Troccoli, A., Fordham, R., & Methven, J. (2011). The impact of large scale atmospheric circulation patterns on wind power generation and its potential predictability: A case study over the UK. *Renewable Energy*, 36(8), 2087–2096. <https://doi.org/10.1016/j.renene.2011.01.025>
- Cassou, C. (2008). Intraseasonal interaction between the Madden-Julian Oscillation and the North Atlantic Oscillation. *Nature*, 455(7212), 523–527. <https://doi.org/10.1038/nature07286>
- Colantuono, G., Wang, Y., Hanna, E., & Erdélyi, R. (2014). Signature of the North Atlantic Oscillation on British solar radiation availability and PV potential: The winter zonal seesaw. *Solar Energy*, 107, 210–219. <https://doi.org/10.1016/j.solener.2014.05.045>
- Dawson, A. (2016). eof: A Library for EOF Analysis of Meteorological, Oceanographic, and Climate Data. *Journal of Open Research Software*, 4, 4–7. <https://doi.org/10.5334/jors.122>
- Drücke, J., Borsche, M., James, P., Kaspar, F., Pfeifroth, U., Ahrens, B., & Trentmann, J. (2020). Climatological analysis of solar and wind energy in Germany using the Grosswetterlagen classification. *Renewable Energy*, 164, 1254–1266. <https://doi.org/10.1016/j.renene.2020.10.102>
- Ely, C. R., Brayshaw, D. J., Methven, J., Cox, J., & Pearce, O. (2013). Implications of the North Atlantic Oscillation for a UK-Norway Renewable power system. *Energy Policy*, 62, 1420–1427. <https://doi.org/10.1016/j.enpol.2013.06.037>
- Eurostat. (2021). *Supply, transformation and consumption of electricity*. https://ec.europa.eu/eurostat/databrowser/view/nrg_cb_e/default/table?lang=en
- Graabak, I., & Korpås, M. (2016). Variability Characteristics of European Wind and Solar Power Resources—A Review. *Energies*, 9(6), 1–31. <https://doi.org/10.3390/en9060449>
- Grams, C. M., Beerli, R., Pfenninger, S., Staffell, I., & Wernli, H. (2017). Balancing Europe's wind-power output through spatial deployment informed by weather regimes. *Nature Climate Change*, 7(8), 557–562. <https://doi.org/10.1038/nclimate3338>
- Hennermann, K., & Yang, X. (2018). *ERA5 data documentation*. European Centre for Medium-Range Weather Forecasts. <https://confluence.ecmwf.int/display/CKB/ERA5+data+documentation>
- Hersbach, H., Bell, B., Berrisford, P., Biavati, G., Horányi, A., Muñoz Sabater, J., Nicolas, J., Peubey, C., Radu, R., Rozum, I., Schepers, D., Simmons, A., Soci, C., Dee, D., & Thépaut, J.-N. (2018). *ERA5 hourly data on pressure levels from 1979 to present*. Copernicus Climate Change Service (C3S) Climate Data Store (CDS). <https://doi.org/10.24381/cds.bd0915c6>
- Hirth, L., & Ziegenhagen, I. (2015). Balancing power and variable renewables: Three links. *Renewable and Sustainable Energy Reviews*, 50(October 2015), 1035–1051. <https://doi.org/10.1016/j.rser.2015.04.180>
- Huld, T., Gottschalg, R., Beyer, H. G., & Topič, M. (2010). Mapping the performance of PV modules, effects of module type and data averaging. *Solar Energy*, 84(2), 324–338. <https://doi.org/10.1016/j.solener.2009.12.002>
- Hulme, M. (2016). 1.5 °C and climate research after the Paris Agreement. *Nature Climate Change*, 6(3), 222–224. <https://doi.org/10.1038/nclimate2939>
- Hurrell, J. W., Kushnir, Y., Ottersen, G., & Visbeck, M. (2003). An overview of the north atlantic oscillation. *Geophysical Monograph Series*, 134, 1–35. <https://doi.org/10.1029/134GM01>
- IRENA. (2020a). *Global Renewables Outlook: Energy transformation 2050*, International Renewable Energy Agency (IRENA), Abu Dhabi.
- IRENA. (2020b). *Renewable capacity statistics 2020*, International Renewable Energy Agency (IRENA), Abu Dhabi.
- Jäger-Waldau, A. (2019). PV Status Report 2019. In EUR 29938 EN, Publications Office of the European Union. <https://doi.org/10.2760/326629>
- Jakubcionis, M., & Carlsson, J. (2017). Estimation of European Union residential sector space cooling potential. *Energy Policy*,

- 101(May 2016), 225–235. <https://doi.org/10.1016/j.enpol.2016.11.047>
- Jerez, S., Trigo, R. M., Vicente-Serrano, S. M., Pozo-Vázquez, D., Lorente-Plazas, R., Lorenzo-Lacruz, J., Santos-Alamillos, F., & Montávez, J. P. (2013). The impact of the north atlantic oscillation on renewable energy resources in Southwestern Europe. *Journal of Applied Meteorology and Climatology*, 52(10), 2204–2225. <https://doi.org/10.1175/JAMC-D-12-0257.1>
- Jones, S., Lee, S. R., & Bloomfield, H. (2020). *Wintertime Impacts of Synoptic-Scale Weather Patterns on the European Energy Sector* (Issue August). University of Reading.
- Lauret, P., Boland, J., & Ridley, B. (2013). Bayesian statistical analysis applied to solar radiation modelling. *Renewable Energy*, 49, 124–127. <https://doi.org/10.1016/j.renene.2012.01.049>
- Michelangeli, P. A., Vautard, R., & Legras, B. (1995). Weather regimes: recurrence and quasi stationarity. In *Journal of the Atmospheric Sciences* (Vol. 52, Issue 8, pp. 1237–1256). [https://doi.org/10.1175/1520-0469\(1995\)052<1237:WRRAQS>2.0.CO;2](https://doi.org/10.1175/1520-0469(1995)052<1237:WRRAQS>2.0.CO;2)
- Muñoz Sabater, J. (2019). *ERA5-Land hourly data from 1981 to present*. Copernicus Climate Change Service (C3S) Climate Data Store (CDS). <https://doi.org/10.24381/cds.e2161bac>
- Pedregosa, F., Varoquaux, G., Gramfort, A., Michel, V., Thirion, B., Grisel, O., Blondel, M., Prettenhofer, P., Weiss, R., Dubourg, V., Vanderplas, J., Passos, A., Cournapeau, D., Brucher, M., Perrot, M., & Duchesnay, E. (2011). Scikit-learn: Machine Learning in {P}ython. *Journal of Machine Learning Research*, 12, 2825–2830.
- Pfenninger, S., & Staffell, I. (2016). Long-term patterns of European PV output using 30 years of validated hourly reanalysis and satellite data. *Energy*, 114, 1251–1265. <https://doi.org/10.1016/j.energy.2016.08.060>
- Pozo-Vázquez, D., Santos-Alamillos, F. J., Lara-Fanego, V., Ruiz-Arias, J. A., & Tovar-Pescador, J. (2011). Hydrological, Socioeconomic and Ecological Impacts of the North Atlantic Oscillation in the Mediterranean Region. In *Hydrological, Socioeconomic and Ecological Impacts of the North Atlantic Oscillation in the Mediterranean Region* (Vol. 46, Issue December 2015). <https://doi.org/10.1007/978-94-007-1372-7>
- Pozo-Vázquez, D., Tovar-Pescador, J., Gámiz-Fortis, S. R., Esteban-Parra, M. J., & Castro-Díez, Y. (2004). NAO and solar radiation variability in the European North Atlantic region. *Geophysical Research Letters*, 31(5), n/a-n/a. <https://doi.org/10.1029/2003gl018502>
- Ram, M., Bogdanov, D., Aghahosseini, A., Oyewo, S., Gulagi, A., Child, M., & Breyer, C. (2017). *Global Energy System based on 100% Renewable Energy – Power Sector. Study by Lappeenranta University of Technology and Energy Watch Group*.
- Ridley, B., Boland, J., & Lauret, P. (2010). Modelling of diffuse solar fraction with multiple predictors. *Renewable Energy*, 35(2), 478–483. <https://doi.org/10.1016/j.renene.2009.07.018>
- Rogers, J. C. (1997). North Atlantic storm track variability and its association to the North Atlantic oscillation and climate variability of Northern Europe. *Journal of Climate*, 10(7), 1635–1647. [https://doi.org/10.1175/1520-0442\(1997\)010<1635:NASTVA>2.0.CO;2](https://doi.org/10.1175/1520-0442(1997)010<1635:NASTVA>2.0.CO;2)
- SolarPower Europe and LUT University. (2020). *100% Renewable Europe - How to make Europe's energy system climate-neutral before 2050*. 64.
- Stram, B. N. (2016). Key challenges to expanding renewable energy. *Energy Policy*, 96, 728–734. <https://doi.org/10.1016/j.enpol.2016.05.034>
- Tröndle, T., Pfenninger, S., & Lilliestam, J. (2019). Home-made or imported: On the possibility for renewable electricity autarky on all scales in Europe. *Energy Strategy Reviews*, 26(June), 100388. <https://doi.org/10.1016/j.esr.2019.100388>
- van der Wiel, K., Bloomfield, H. C., Lee, R. W., Stoop, L. P., Blackport, R., Screen, J. A., & Selten, F. M. (2019). The influence of weather regimes on European renewable energy production and demand. *Environmental Research Letters*, 14(9), 094010. <https://doi.org/10.1088/1748-9326/ab38d3>
- Vautard, R. (1990). Multiple weather regimes over the North Atlantic: analysis of precursors and successors. *Monthly Weather Review*, 118(10). [https://doi.org/10.1175/1520-0493\(1990\)118<2056:MWROTN>2.0.CO;2](https://doi.org/10.1175/1520-0493(1990)118<2056:MWROTN>2.0.CO;2)
- Virtanen, P., Gommers, R., Oliphant, T. E., Haberland, M., Reddy, T., Cournapeau, D., Burovski, E., Peterson, P., Weckesser, W., Bright, J., van der Walt, S. J., Brett, M., Wilson, J., Millman, K. J., Mayorov, N., Nelson, A. R. J., Jones, E., Kern, R., Larson, E., ... SciPy 1.0 Contributors. (2020). SciPy 1.0: Fundamental Algorithms for Scientific Computing in Python. *Nature Methods*, 17, 261–272. <https://doi.org/10.1038/s41592-019-0686-2>
- Wallace, J. M., & Hobbs, P. V. (2006). *Atmospheric Science: An Introductory Survey* (2nd ed.). Amsterdam ; Boston : Elsevier Academic Press, [2006].
- Wiese, F., Schlecht, I., Bunke, W. D., Gerbaulet, C., Hirth, L., Jahn, M., Kunz, F., Lorenz, C., Mühlendorf, J., Reimann, J., & Schill, W. P. (2019). Open Power System Data – Frictionless data for electricity system modelling. *Applied Energy*, 236(June 2018), 401–409. <https://doi.org/10.1016/j.apenergy.2018.11.097>

7. Appendix

All scripts and figures used in this study can be found in the following GitHub repository:
<https://github.com/dirk7744/RPGV>.

Table 8: The defined seven weather regimes and no regime and their frequency throughout the season.

| | Winter (DJF) | Spring (MAM) | Summer (JJA) | Autumn (SON) |
|------------------|--------------|--------------|--------------|--------------|
| WR0 | 19.4% | 13.7% | 12.6% | 12.4% |
| WR1 | 11.9% | 16.0% | 14.5% | 16.4% |
| WR2 | 13.9% | 10.1% | 6.2% | 9.1% |
| WR3 | 13.9% | 12.5% | 15.6% | 16.6% |
| WR4 | 9.7% | 14.3% | 17.6% | 11.7% |
| WR5 | 14.0% | 13.3% | 14.1% | 12.6% |
| WR6 | 11.4% | 13.1% | 11.8% | 14.1% |
| no regime | 5.8% | 7.0% | 7.5% | 7.0% |

Table 9: Current (2019) and projected (2030) PV power production anomaly (difference to the seasonal mean) estimates per weather regime and season. The projection to 2030 is based on the National Energy and climate plans (NECPs). Framed in blue are the lowest anomalies per season, and framed in red are the highest anomalies per season.

| | | PV power production anomaly 2019 (GW) | PV power production anomaly 2030 (GW) |
|---|------------------|--|--|
| <u>Winter</u> Mean production: 8.6 GW | WR0 | -0.36 | -0.74 |
| | WR1 | -0.89 | -2.87 |
| | WR2 | -0.08 | -0.55 |
| | WR3 | 0.55 | 2.26 |
| | WR4 | -0.87 | -2.52 |
| | WR5 | 0.62 | 1.68 |
| | WR6 | 0.77 | 1.87 |
| <u>Spring</u> Mean production: 21.7 GW | no regime | 0.52 | 1.15 |
| | WR0 | -0.74 | -1.80 |
| | WR1 | -1.43 | -4.11 |
| | WR2 | -0.78 | -2.49 |
| | WR3 | 0.25 | 1.24 |
| | WR4 | 0.36 | 1.02 |
| | WR5 | 1.53 | 4.12 |
| <u>Summer</u> Mean production: 25.7 GW | WR6 | 0.97 | 2.40 |
| | no regime | 0.05 | 0.36 |
| | WR0 | 0.18 | 0.42 |
| | WR1 | -0.78 | -2.15 |
| | WR2 | -0.63 | -1.92 |
| | WR3 | -0.16 | -0.24 |
| | WR4 | 0.13 | 0.36 |
| <u>Autumn</u> Mean production: 14.0 GW | WR5 | 0.98 | 2.74 |
| | WR6 | 0.19 | 0.47 |
| | no regime | -0.18 | -0.49 |
| | WR0 | -1.00 | -2.72 |
| | WR1 | -1.41 | -4.18 |
| | WR2 | -0.68 | -2.30 |
| | WR3 | 0.82 | 2.65 |

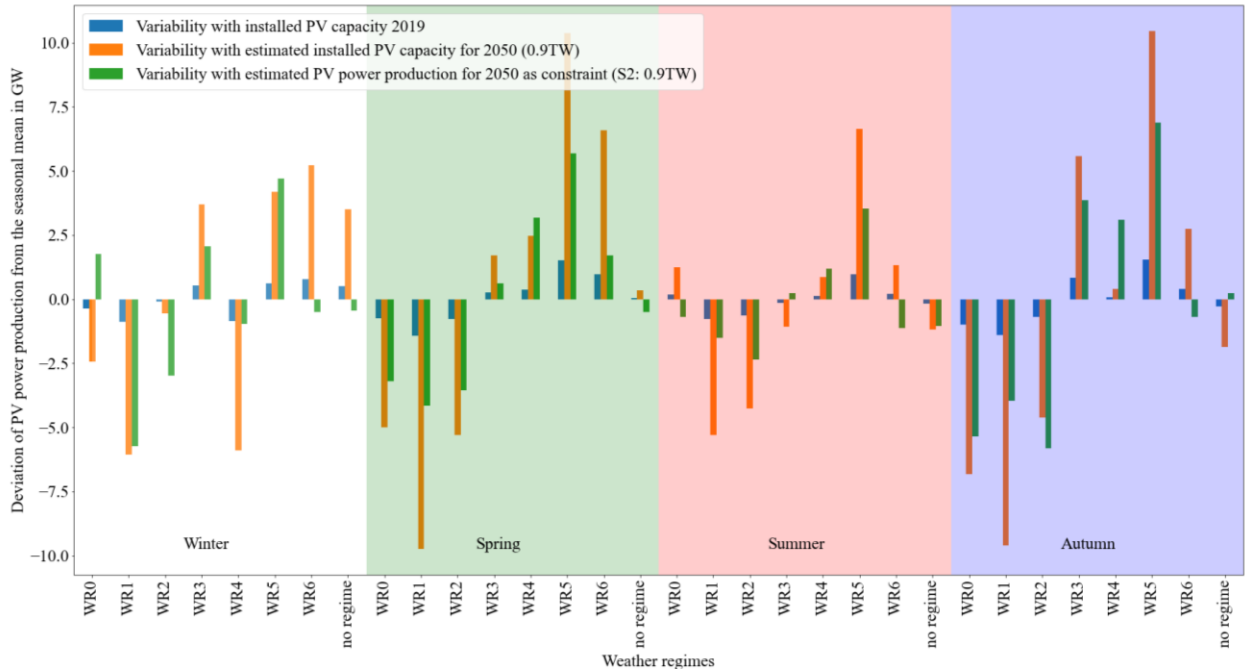


Figure 17: Deviation of the PV power production from the seasonal mean per weather regime and season. In blue the variability for the current situation (2019), in orange the estimated variability with the upscaled installed capacities to the year 2050 (0.9 TW) and in green the estimated variability with the installed capacity distribution for scenario 2-1.

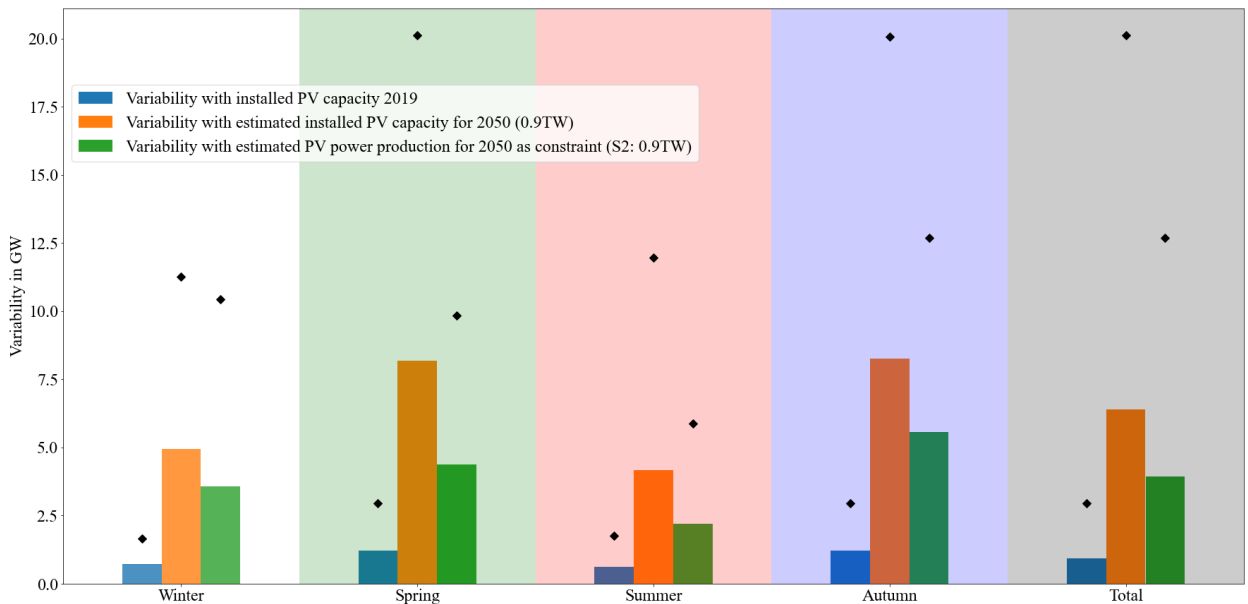


Figure 18: Mean (bars) and maximum (black markers) consolidated (over all weather regimes) variability per season and overall (total). In blue the variability for the current situation (2019), in orange the estimated variability with the upscaled installed capacities to the year 2050 (0.9 TW) and in green the estimated variability with the installed capacity distribution for scenario 2-1.

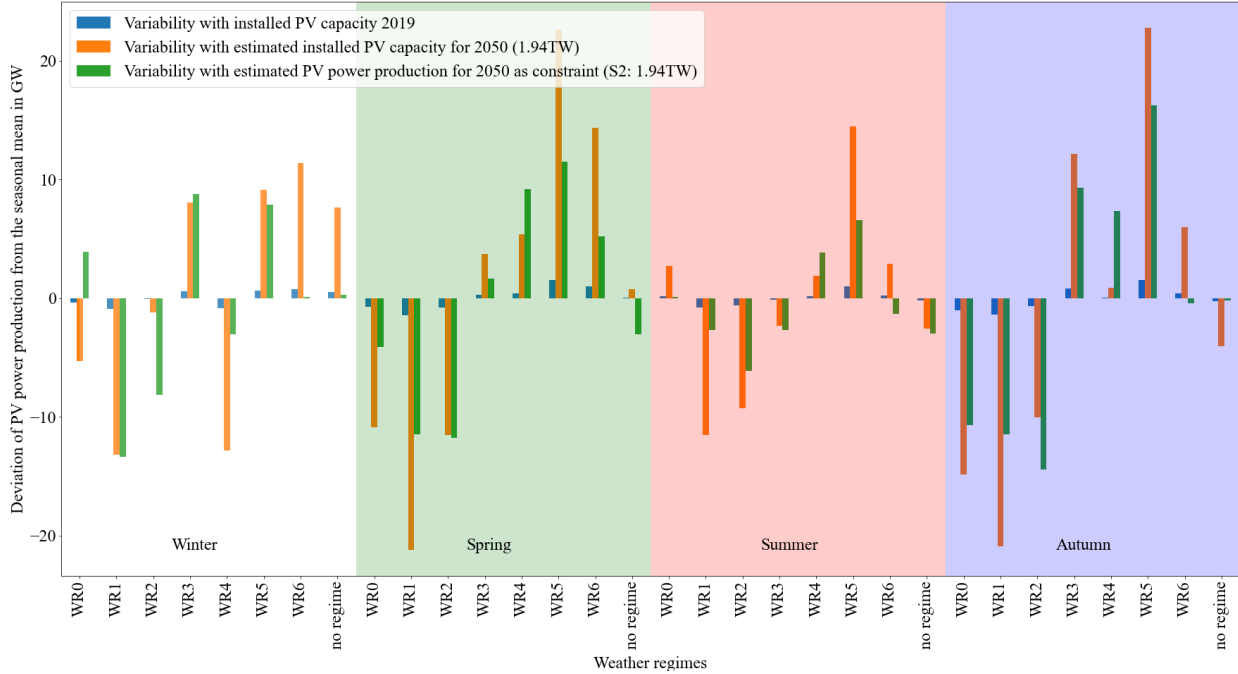


Figure 19: Deviation of the PV power production from the seasonal mean per weather regime and season. In blue the variability for the current situation (2019), in orange the estimated variability with the upscaled installed capacities to the year 2050 (1.94 TW) and in green the estimated variability with the installed capacity distribution for scenario 2-2.

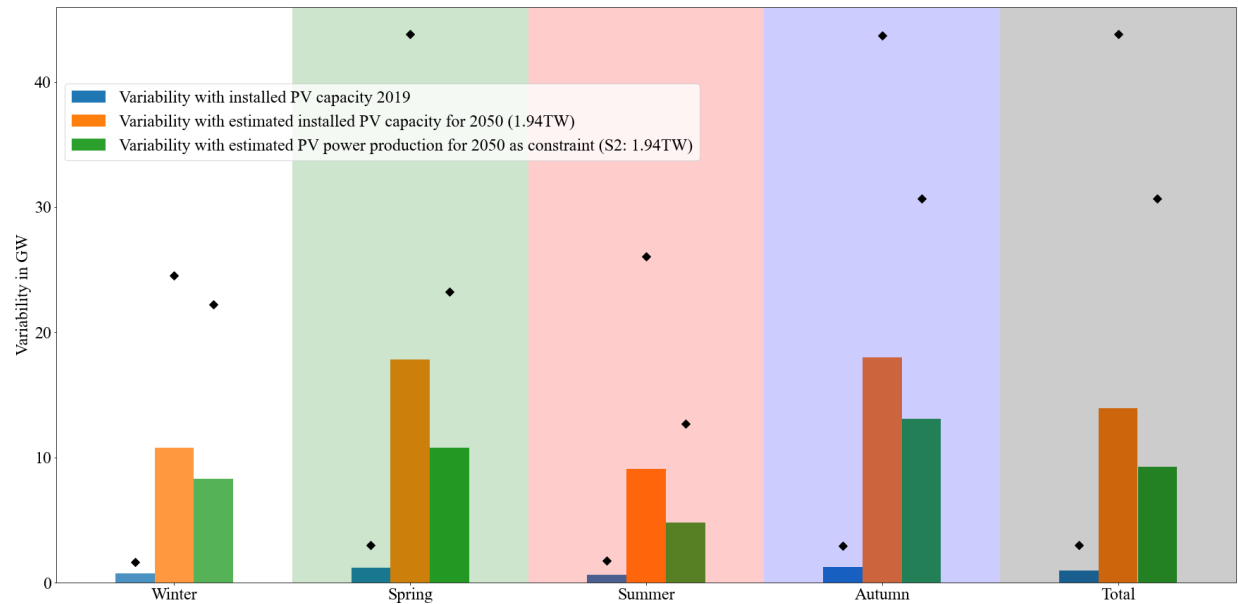


Figure 20: Mean (bars) and maximum (black markers) consolidated (over all weather regimes) variability per season and overall (total). In blue the variability for the current situation (2019), in orange the estimated variability with the upscaled installed capacities to the year 2050 (1.94 TW) and in green the estimated variability with the installed capacity distribution for scenario 2-2.

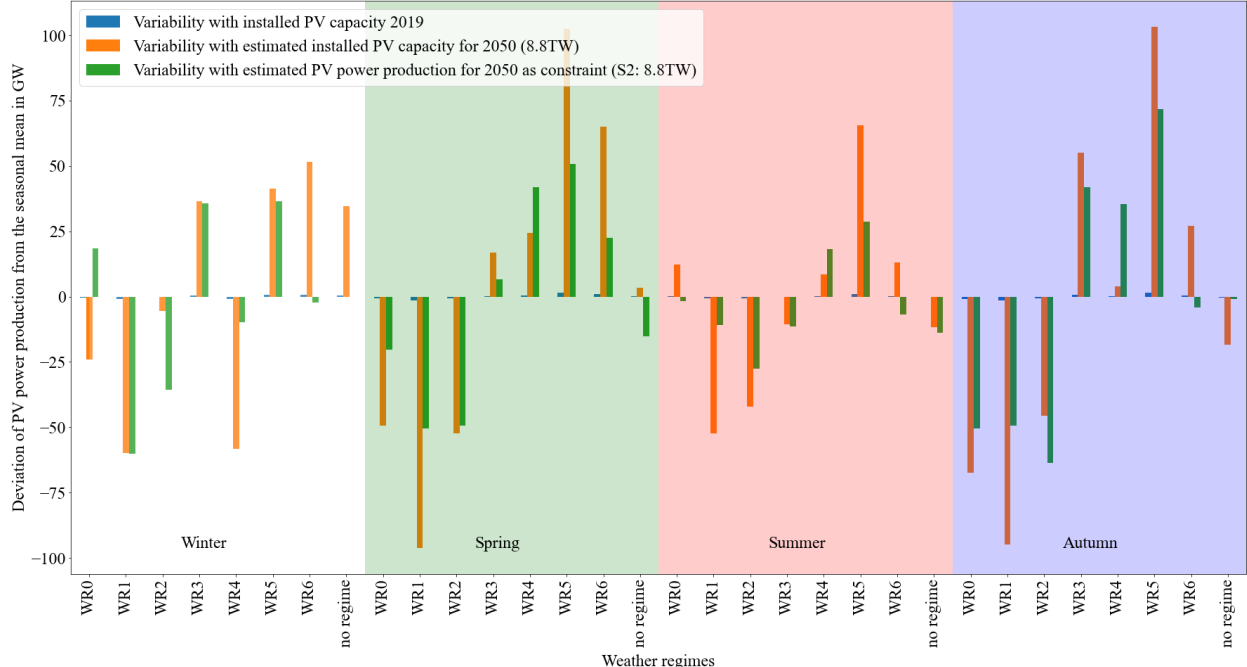


Figure 21: Deviation of the PV power production from the seasonal mean per weather regime and season. In blue the variability for the current situation (2019), in orange the estimated variability with the upscaled installed capacities to the year 2050 (8.8 TW) and in green the estimated variability with the installed capacity distribution for scenario 2-3.

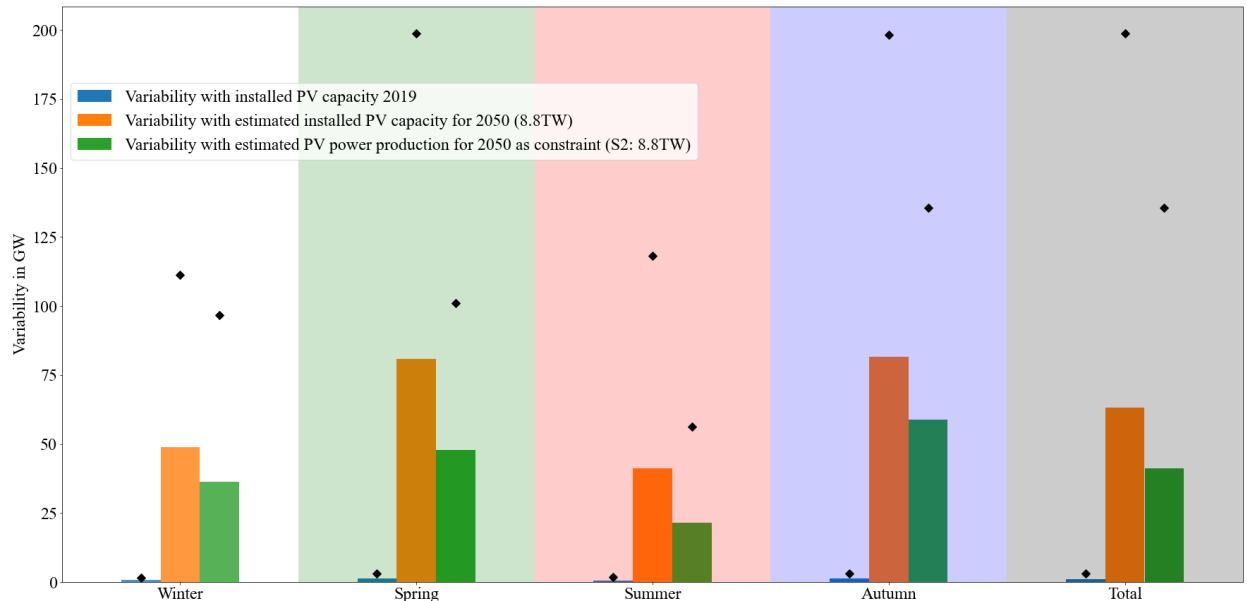


Figure 22: Mean (bars) and maximum (black markers) consolidated (over all weather regimes) variability per season and overall (total). In blue the variability for the current situation (2019), in orange the estimated variability with the upscaled installed capacities to the year 2050 (8.8 TW) and in green the estimated variability with the installed capacity distribution for scenario 2-3.

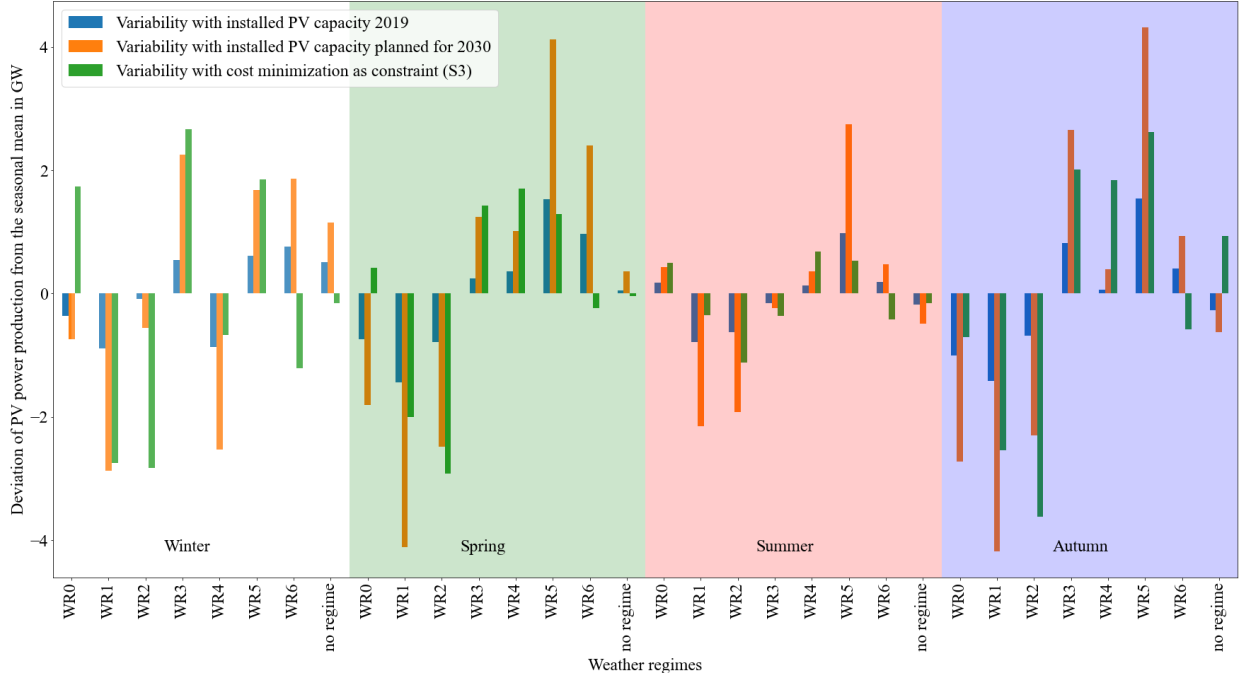


Figure 23: Deviation of the PV power production from the seasonal mean per weather regime and season. In blue the variability for the current situation (2019), in orange the estimated variability with the planned installed capacities for 2030 (NECPs) and in green the estimated variability with the installed capacity distribution for scenario 3-1.

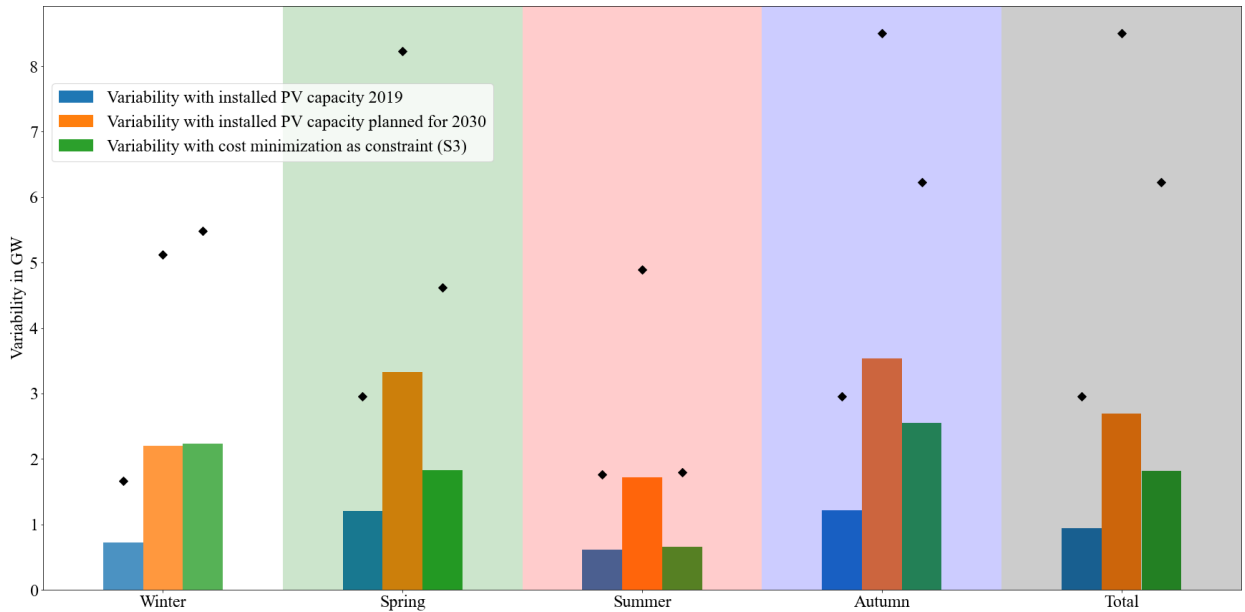


Figure 24: Mean (bars) and maximum (black markers) consolidated (over all weather regimes) variability per season and overall (total). In blue the variability for the current situation (2019), in orange the estimated variability with the planned installed capacities for 2030 (NECPs) and in green the estimated variability with the installed capacity distribution for scenario 3-1.

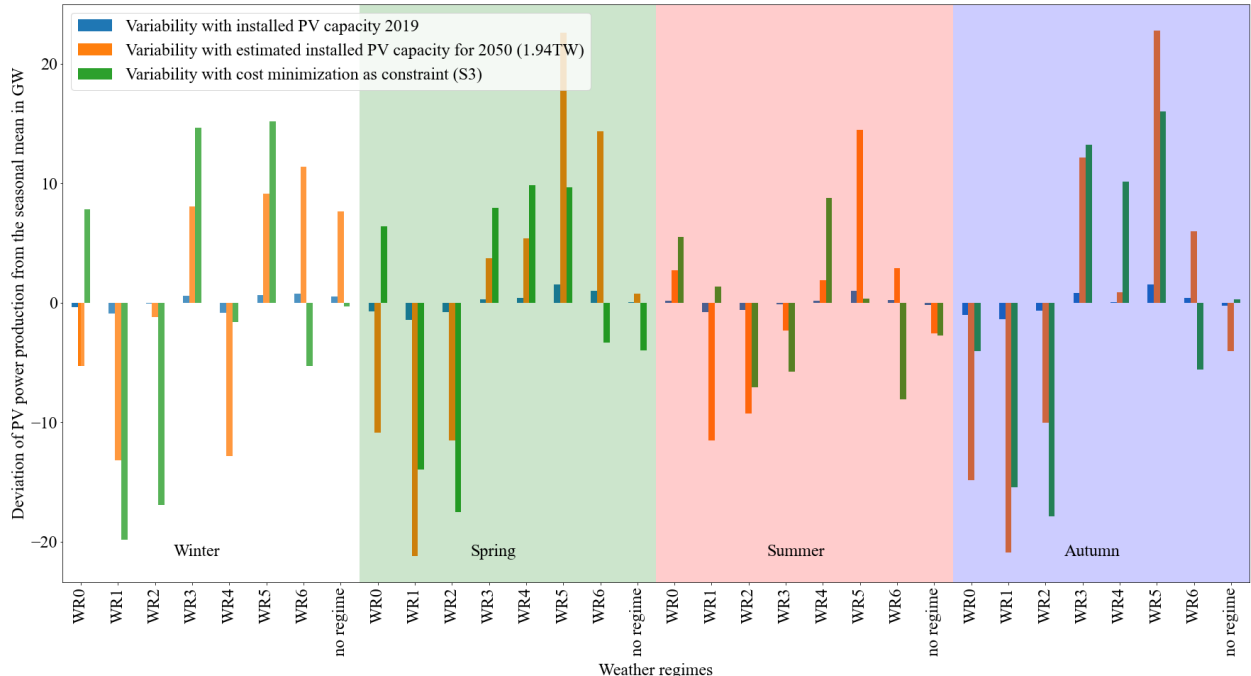


Figure 25: Deviation of the PV power production from the seasonal mean per weather regime and season. In blue the variability for the current situation (2019), in orange the estimated variability with the upscaled installed capacities to the year 2050 (1.94 TW) and in green the estimated variability with the installed capacity distribution for scenario 3-2.

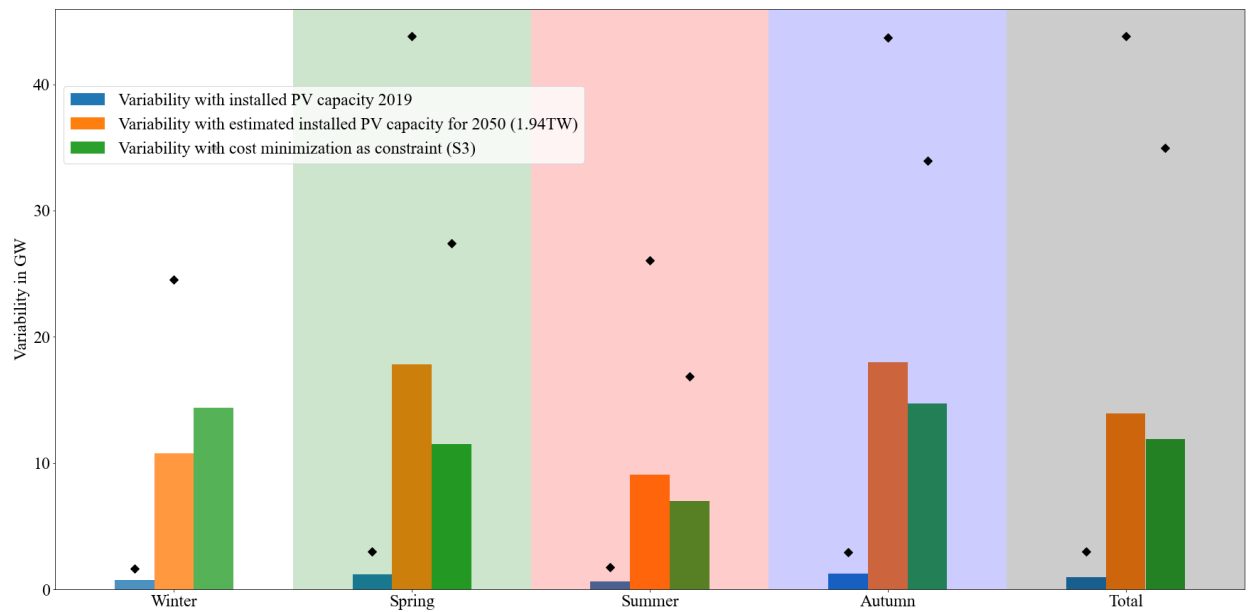


Figure 26: Mean (bars) and maximum (black markers) consolidated (over all weather regimes) variability per season and overall (total). In blue the variability for the current situation (2019), in orange the estimated variability with the upscaled installed capacities to the year 2050 (1.94 TW) and in green the estimated variability with the installed capacity distribution for scenario 3-2.

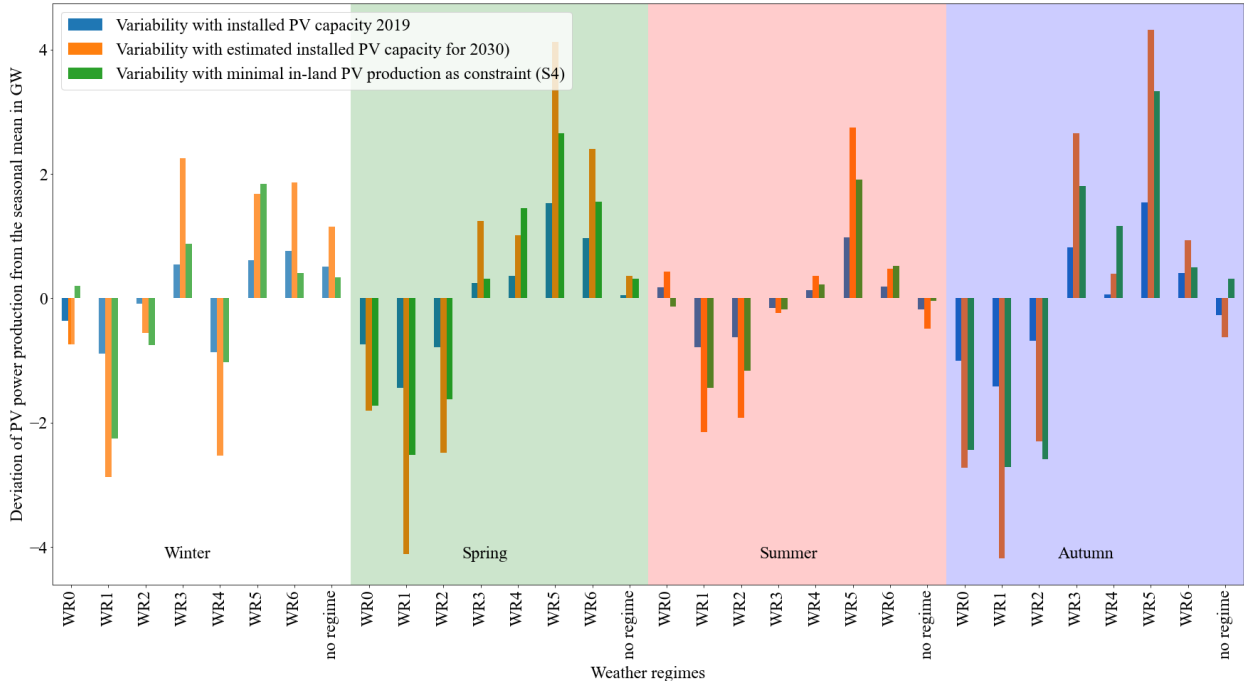


Figure 27: Deviation of the PV power production from the seasonal mean per weather regime and season. In blue the variability for the current situation (2019), in orange the estimated variability with the planned installed capacities for 2030 (NECPs) and in green the estimated variability with the installed capacity distribution for scenario 4-1.

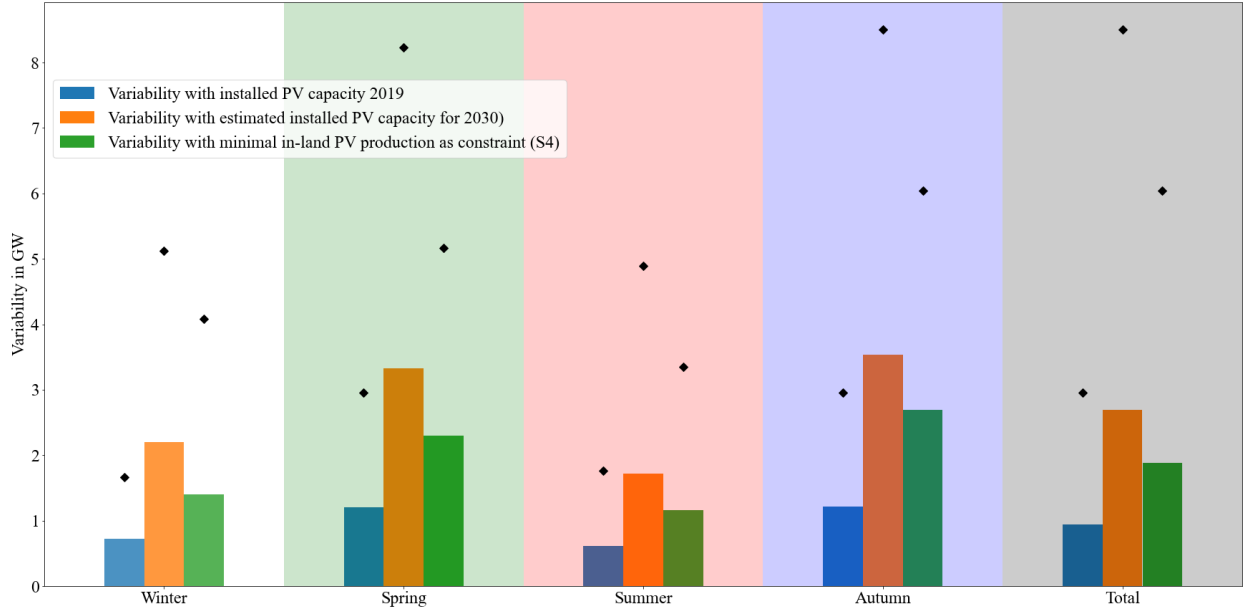


Figure 28: Mean (bars) and maximum (black markers) consolidated (over all weather regimes) variability per season and overall (total). In blue the variability for the current situation (2019), in orange the estimated variability with the planned installed capacities for 2030 (NECPs) and in green the estimated variability with the installed capacity distribution for scenario 4-1.

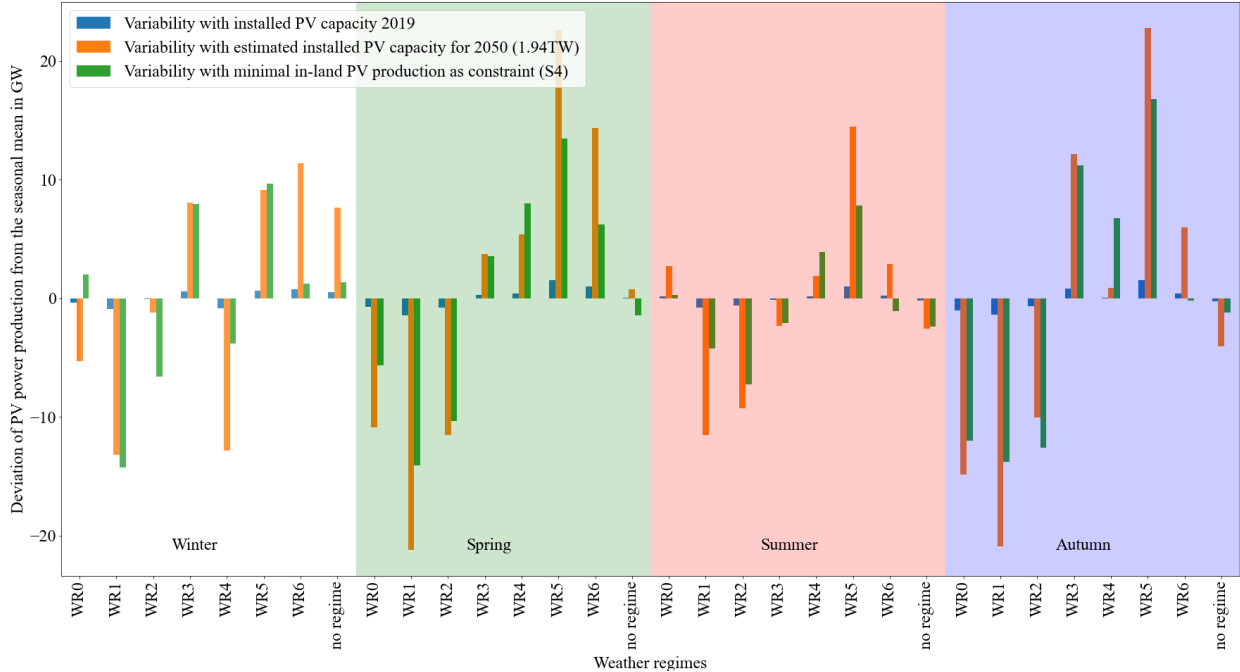


Figure 29: Deviation of the PV power production from the seasonal mean per weather regime and season. In blue the variability for the current situation (2019), in orange the estimated variability with the upscaled installed capacities to the year 2050 (1.94 TW) and in green the estimated variability with the installed capacity distribution for scenario 4-2.

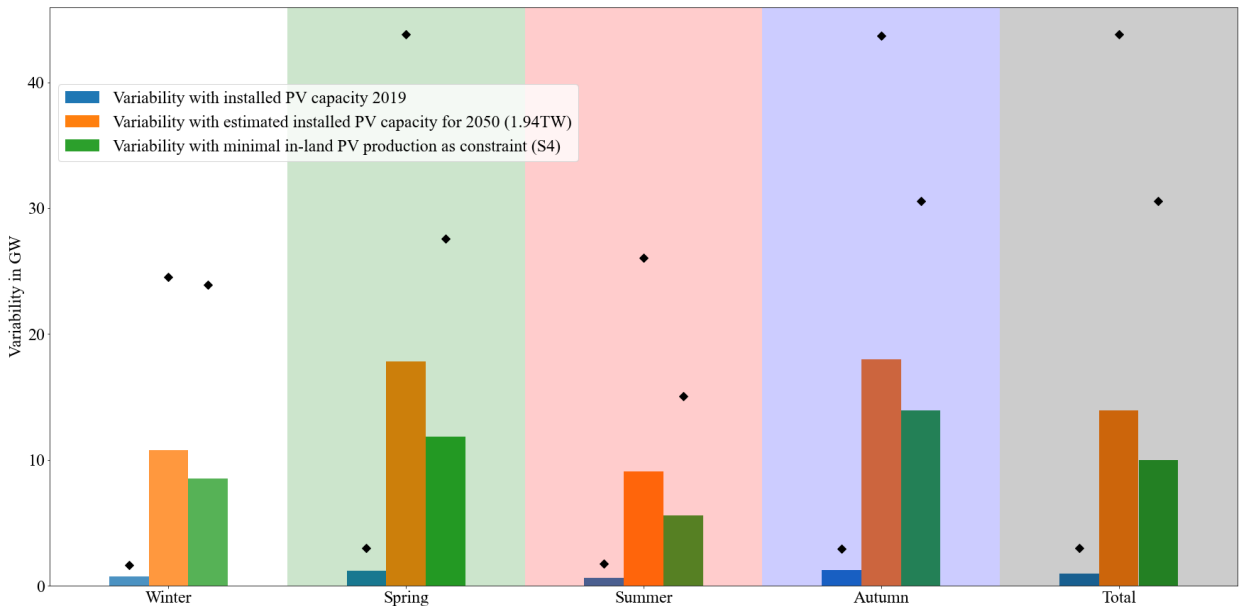


Figure 30: Mean (bars) and maximum (black markers) consolidated (over all weather regimes) variability per season and overall (total). In blue the variability for the current situation (2019), in orange the estimated variability with the upscaled installed capacities to the year 2050 (1.94 TW) and in green the estimated variability with the installed capacity distribution for scenario 4-2.

Declaration of originality

The signed declaration of originality is a component of every semester paper, Bachelor's thesis, Master's thesis and any other degree paper undertaken during the course of studies, including the respective electronic versions.

Lecturers may also require a declaration of originality for other written papers compiled for their courses.

I hereby confirm that I am the sole author of the written work here enclosed and that I have compiled it in my own words. Parts excepted are corrections of form and content by the supervisor.

Title of work (in block letters):

How to Distribute New Solar Systems in Europe to Reduce Power Production Variability

Authored by (in block letters):

For papers written by groups the names of all authors are required.

Name(s):

Mühlemann

First name(s):

Dirk

With my signature I confirm that

- I have committed none of the forms of plagiarism described in the '[Citation etiquette](#)' information sheet.
- I have documented all methods, data and processes truthfully.
- I have not manipulated any data.
- I have mentioned all persons who were significant facilitators of the work.

I am aware that the work may be screened electronically for plagiarism.

Place, date

Uster, 23/04/2021

Signature(s)



For papers written by groups the names of all authors are required. Their signatures collectively guarantee the entire content of the written paper.